Cell Reports

Article

Single-cell RNA-seq-based proteogenomics identifies glioblastoma-specific transposable elements encoding HLA-I-presented peptides

Graphical abstract

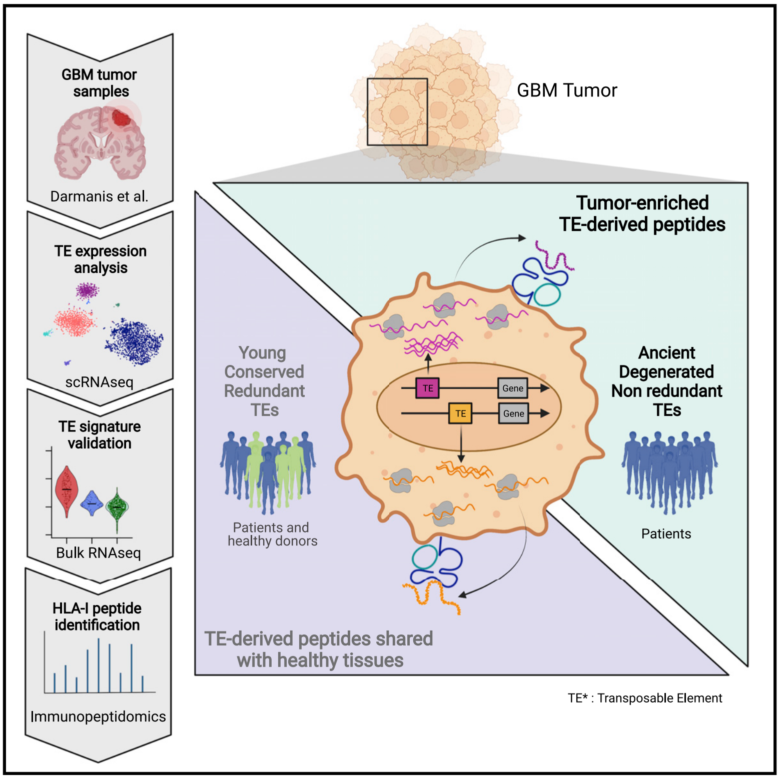

Highlights

- Transposable elements (TEs) allow all cell population discrimination in glioblastoma
- TE-derived peptides are presented on HLA-I molecules
- TE subfamilies redundantly share HLA-I-presented peptide coding sequences
- Non-redundant peptide-coding TEs are more tumor-specific targets for immunotherapy

Authors

Pierre-Emmanuel Bonté, Yago A. Arribas, Antonela Merlotti, ..., Cécile Alanio, Christel Goudot, Sebastian Amigorena

Correspondence

christel.goudot@curie.fr (C.G.), sebastian.amigorena@curie.fr (S.A.)

In brief

Bonté et al. combine and analyze single-cell and bulk transcriptomic samples with immunopeptidomic datasets to identify glioblastoma HLA-I peptide-coding transposable elements. Some peptides are encoded by single copies of transposable elements from old subfamilies and represent potential tumor-specific targets for cancer immunotherapies.

Bonté et al., 2022, Cell Reports 39, 110916
June 7, 2022
https://doi.org/10.1016/j.celrep.2022.110916

Cell Reports

CellPress
OPEN ACCESS

Article

Single-cell RNA-seq-based proteogenomics identifies glioblastoma-specific transposable elements encoding HLA-I-presented peptides

Pierre-Emmanuel Bonté,[1,6] Yago A. Arribas,[1,6] Antonela Merlotti,[1] Montserrat Carrascal,[2] Jiasi Vicky Zhang,[3] Elina Zueva,[1] Zev A. Binder,[3] Cécile Alanio,[1,4,5] Christel Goudot,[1,7,*] and Sebastian Amigorena[1,7,8,*]

[1]Institut Curie, PSL University, INSERM U932, Immunity and Cancer, 75005 Paris, France

[2]Biological and Environmental Proteomics, Institut d'Investigacions Biomèdiques de Barcelona-CSIC, IDIBAPS, Roselló 161, 6a planta, 08036 Barcelona, Spain

[3]GBM Translational Center of Excellence, Department of Neurosurgery, Perelman School of Medicine, University of Pennsylvania, Philadelphia, PA 19104, USA

[4]Laboratoire d'Immunologie Clinique, Institut Curie, Paris 75005, France

[5]Parker Institute of Cancer Immunotherapy, San Francisco, CA, USA

[6]These authors contributed equally

[7]These authors contributed equally

[8]Lead contact

*Correspondence: christel.goudot@curie.fr (C.G.), sebastian.amigorena@curie.fr (S.A.)

https://doi.org/10.1016/j.celrep.2022.110916

SUMMARY

We analyze transposable elements (TEs) in glioblastoma (GBM) patients using a proteogenomic pipeline that combines single-cell transcriptomics, bulk RNA sequencing (RNA-seq) samples from tumors and healthy-tissue cohorts, and immunopeptidomic samples. We thus identify 370 human leukocyte antigen (HLA)-I-bound peptides encoded by TEs differentially expressed in GBM. Some of the peptides are encoded by repeat sequences from intact open reading frames (ORFs) present in up to several hundred TEs from recent long interspersed nuclear element (LINE)-1, long terminal repeat (LTR), and SVA subfamilies. Other HLA-I-bound peptides are encoded by single copies of TEs from old subfamilies that are expressed recurrently in GBM tumors and not expressed, or very infrequently and at low levels, in healthy tissues (including brain). These peptide-coding, GBM-specific, highly recurrent TEs represent potential tumor-specific targets for cancer immunotherapies.

INTRODUCTION

T cells can control, and sometimes reject, solid tumors, especially after reprogramming by immune checkpoint blockade (ICB) (Morotti et al., 2021; Waldman et al., 2020). The nature of the tumor antigens targeted by these T cells, however, remains unclear. After identification of differentiation and tumor-testis antigens decades ago (Almeida et al., 2009; Boon and van der Bruggen, 1996; Simpson et al., 2005; van der Bruggen et al., 1991), a new family of antigens derived from tumor somatic mutations was discovered (Coulie et al., 1995; Robbins et al., 1996; Tran et al., 2015; van Rooij et al., 2013). Defined sets of mutations in single cells, occurring before or after oncogenic transformation, are amplified by clonal expansion of tumor cells (Castle et al., 2012). This "amplified" set of mutations becomes "visible" to the immune system and triggers T cell immune responses (Lennerz et al., 2005; Robbins et al., 2013; van Rooij et al., 2013). Unlike differentiation and tumor testis antigens that are, by definition, also expressed in certain normal cells, mutational neo-antigens are strictly tumor specific. However, most such mutations are passenger events and are largely specific to individual patients. The presence of mutation-specific T cells in ICB-treated cancer patients, the high rate of clinical responses to ICB in patients with microsatellite instability, and the correlation between the median number of mutations in certain cancer types and the rate of response to ICB, all indicate that passenger mutations can be effectively targeted by T cells in cancer patients (Carreno et al., 2015; Chauvin et al., 2015; Gubin et al., 2014; Le et al., 2015; Rizvi et al., 2015; Schadendorf et al., 2015; Snyder et al., 2014).

Several lines of evidence, however, also suggest that point mutations are not the only antigens seen by T cells on human tumors. First, there are exceptions to the correlation between the frequency of mutations and the rates of response to ICB (McGrail et al., 2021). Renal cell carcinoma (RCC), for example, has a mutational burden around two mutations per megabase (MB) and a response rate to ICB around 25%, as compared with squamous non-small cell lung cancer (LUSC), with around nine mutations/MB and a response rate to ICB of 17% (Yarchoan et al., 2017, 2019). Second, at the level of individual patients, the number of mutations is not highly predictive of clinical responses to ICB (Gromeier et al., 2021; McGrail et al., 2021). Finally, there

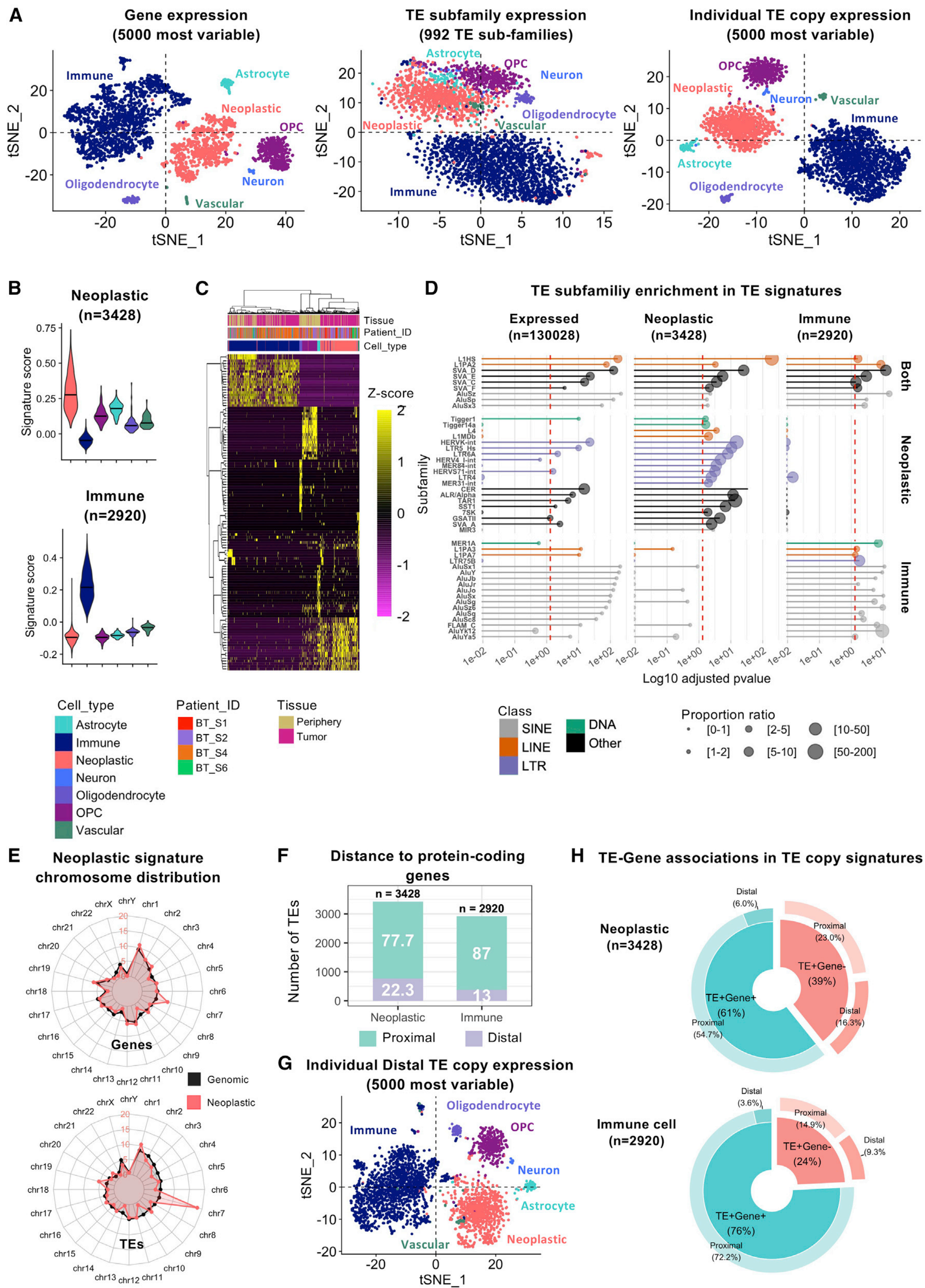

(legend on next page)

are multiple examples in the literature of T cell responses to non-mutational antigens in cancer patients, including differentiation and tumor-testis antigens (Novellino et al., 2005; Rapoport et al., 2015; Rooney et al., 2015).

Different teams have recently used proteogenomic approaches to search broadly for tumor-specific, non-canonical open reading frames (ORFs) that encode peptides presented by human leukocyte antigen (HLA)-I molecules on tumor cells (Chong et al., 2020; Laumont et al., 2016). Most of the identified peptides in these studies derive from non-coding genomic regions. Some of these potential tumor-specific antigens are found in multiple patients and can induce immune responses *in vitro* or in mouse models (Ehx et al., 2021; Laumont et al., 2018). A large fraction of the non-coding genome is composed of transposable elements (TEs). TEs include DNA transposons (Burns, 2017) as well as three main classes of retrotransposons (short interspersed nuclear elements [SINEs], long interspersed nuclear elements [LINEs], and long terminal repeats [LTRs]). Each class is sub-divided into families and subfamilies that arose during evolution from common ancestors and are classified according to sequence homology of the individual copies in the genome. The age of TE subfamilies can be estimated based on the conservation of their repeat motifs (Choudhary et al., 2020). A small proportion of young LINE-1 in the human genome can still be active for retro-transposition (Lanciano and Cristofari, 2020; Zhao et al., 2020). Retro-transposition can compromise the stability of the genome, and mammalian differentiated cells in tissues protect themselves against TE-induced genome instability through epigenetic repression of TE transcription (Burns, 2017; Slotkin and Martienssen, 2007). As a result, TE transcription is low in most adult cells and more active during embryonic development, in stem cells and, intriguingly, in tumors (Garcia-Perez et al., 2016). TE de-repression in tumors occurs through multiple epigenetic changes to TE loci, including DNA and histone demethylation (Anwar et al., 2017; Grundy et al., 2021; Lynch-Sutherland et al., 2020). Both epigenetic changes can be associated with oncogenesis, resulting in different levels of epigenetic de-regulation.

TE overexpression in tumors compared with healthy tissue has prompted multiple teams to search for anti-TE T cell responses in cancer, and there is clear evidence that this can occur (Neukirch et al., 2019; Rycaj et al., 2015; Saini et al., 2020; Wang-Johanning et al., 2008). One recent study showed presentation of TE-derived peptides on HLA-I molecules (Kong et al., 2019). This study, however, only analyzed peptides derived from TE-subfamilies and did not address the cellular origin of the identified HLA-I-presented peptides. Whether TEs de-repressed in tumors can be a source of truly tumor-specific antigens is therefore still an open question. Here, we propose an original TE-centered proteogenomic approach based on a combination of single-cell transcriptomics and bulk RNA sequencing (RNA-seq) analyses in tumor and healthy tissues, together with immunopeptidomics, to identify single and recurrent, tumor-selective TE-derived peptides presented by HLA-I molecules on GBM tumors.

RESULTS

Single-cell TE expression resolves all cell populations in tumors

We reasoned that a powerful way to identify TEs expressed specifically in tumor cells would be to compare TE expression in tumor and in tumor-infiltrating cells from the same patient. To do so, we used single-cell transcriptomics (single-cell RNA-seq [scRNA-seq]) of all cells present in the tumor microenvironment. We initiated the study on a public dataset including tumor and juxta-tumor samples from four GBM patients analyzed by SMARTseq2 (Figure S1A). Consistent with the analysis performed in the original article (Darmanis et al., 2017), dimensionality reduction and t-distributed stochastic neighbor embedding (t-SNE) visualization based on gene expression resolves the seven sorted cell populations from the tumor core and the surrounding tissue (tumor and periphery in Figure S1A): immune cells (mostly macrophages), neoplastic cells, and oligodendrocyte precursor cells (OPCs) are the most numerous (Figures 1A, left panel, and S1B).

To investigate TE expression in single cells, we mapped scRNA-seq reads to either TE subfamilies (as shown previously; Kong et al., 2019) or to individual genomic TEs (Figure S1C). Because mapping of TEs to individual genomic locations can be affected by high conservation of their repeat motifs, we compared the use of uniquely and multi-mapping reads. Uniquely mapping reads allow accurate estimation of the expression of oldest TE subfamilies but underestimate the expression for youngest TE subfamilies, as compared with multi-mapping reads, which reflect more accurately expression of young TE subfamilies (Figure S1D; Lanciano and Cristofari, 2020).

t-SNE based on expression on all 992 TE subfamilies, or 5,000 most variable individual TEs in single cells, like gene expression, resolves all cell populations in the tumor microenvironment (Figure 1A, middle panel). Neoplastic cells and OPCs are mostly present in tumor and juxta-tumor (Figure S1A, right panel) samples, respectively, while immune cells are present in both. Individually

Figure 1. Single-cell TE expression distinguishes cell populations in GBM tumors

(A) t-SNE visualizing all single cells after filtering (n = 3,167) segregated based on gene expression (left), TE subfamily expression (middle), and individual TE copy expression (right). Cells are color coded based on cell population.

(B) Violin plots representing TE-specific signatures for neoplastic cells (top) and immune cells (bottom).

(C) Unsupervised heatmap showing expression of top 20 differentially expressed TEs for each cell population.

(D) Plot showing TE subfamily enrichment analysis using all expressed TEs (left), neoplastic (middle), and immune (right) signatures. Red dashes represent adjusted $p < 0.05$ on x axis.

(E) Radar plots displaying the rate of genes (top) and TEs (bottom) along all chromosomes.

(F) Barplot showing the number of TEs in proximal or distal regions of nearest protein-coding genes in neoplastic and immune signatures.

(G) t-SNE visualizing cell populations using the individual distal TE copy expression.

(H) Plots summarizing the association between TEs and genes described above in neoplastic (top) and immune signatures (bottom).

mapped TEs allow better resolution of the different cell populations than TE subfamilies (Figure 1A, right panel). These results show that expression of individual TEs can be resolved at the single cell level and is sufficient to distinguish different cell populations in the tumor microenvironment.

TE subfamilies are differentially expressed in neoplastic and immune cells

To better understand the nature of these TEs, we performed differential expression (DE) analyses of TEs in each cell population against all others, thus defining population-specific TE signatures (Figure S1E). These signatures are selective for neoplastic cells, immune cells (Figure 1B), and for each of the other cell populations present in the tumor microenvironment (Figure S1F). Heatmap representation of the 20 most differentially expressed TEs based on the average log2 fold change shows selective expression in each cell population, including in neoplastic cells (Figure 1C). To further investigate the nature of the TEs differentially expressed in each cell population, we compared each signature with all TEs expressed in the dataset (130,028). TEs differentially expressed in neoplastic cells are depleted in SINEs (51.7% versus 44.5%) and enriched in LTRs (8.3% versus 12.1%), while TEs in immune cells are depleted in LINEs (30.3% versus 26.5%) and LTRs (8.3% versus 5.6%) and enriched in SINEs (51.7% versus 59.2%) (Figure S2A), confirming the results from direct mapping of TE subfamilies (Figure S2B). Statistical analyses by subfamily show strong enrichment for several LTR subfamilies in neoplastic cells (mainly human endogenous retrovirus [HERV]), while immune cells differentially express several SINE subfamilies (mainly Alu) (Figure 1D). We conclude that the different cell types present in the tumor environment express distinct patterns of TE subfamilies that can be analyzed from individually mapped TEs by single-cell transcriptomics.

Gain of chromosome 7 and loss of chromosome 10 are recurrent genomic copy number alterations in GBM (Kurscheid et al., 2015). As an internal control for TE mapping to chromosomal loci, we quantified genes and TEs in each cell-type-specific signature to their respective chromosomes. As shown in Figure 1E, TEs differentially expressed in neoplastic cells, but not in other cell populations, present a clear bias for chromosome 7 (Figures 1E, S2C, and S2D). The bias for chromosome 7 in neoplastic cells is even stronger for TEs than for genes, while the loss of chromosome 10 is similar in the TE and gene signatures (Figure S2C). A chromosome 7 bias is also observed when considering only the expression of distal TEs, i.e., TEs located at more than 2 Kb from the nearest protein-coding genes (mostly intergenic), indicating that this bias is not due to high contamination with intron retained TEs in the scRNA-seq datasets (Figure S2E). We conclude that individual TEs can be accurately mapped from scRNA-seq and, as expected, show a chromosome 7 bias selectively in neoplastic GBM cells.

TE expression in neoplastic cells is enriched in elements independent of their closest gene

To better understand the control of TE expression in different cell populations, we first analyzed TE genomic locations. As compared with all expressed TEs in the dataset, TEs differentially expressed in neoplastic cells show reduced intronic locations (77% versus 38.7%), including when compared with the proportion of intronic TEs differentially expressed in immune cells (68.8%) or astrocytes (71%) (Figure S2F). Neoplastic Tes also show a marked increase in 3′ UTR encoded TEs (25.3%), compared with all expressed TEs (5%) or with immune cell TEs (11.3%) (Figure S2F). These results show that, while TEs differentially expressed in immune cells are largely intronic, TEs differentially expressed in neoplastic cells are more frequently from intergenic and 3′ UTRs regions.

Consistent with these results, the proportion of distal TEs is higher in the neoplastic cell signature (22.3%) than in the immune cell signature (13%; Figure 1F). t-SNE analysis based on distal TEs resolves all cell populations (Figure 1G), suggesting that cell-type-specific TE expression may not be exclusively due to gene-driven transcription. Consistently, the TE-gene distances are increased for TEs differentially expressed in neoplastic cells, especially for LINEs and LTRs (Figure S2G), as compared with the TEs differentially expressed in immune cells. Higher distances from the closest genes for TEs expressed selectively in neoplastic cells could reflect gene-independent TE expression, including enhancer-dependent or long non-coding (Lnc) RNA-dependent readthrough transcription. We therefore next analyzed the correlation between expression of TEs and their closest genes in neoplastic and immune cells. Figure S2H shows examples of proximal and distal TEs, expressed together or independently of their closest gene. Quantification of the proportions of TEs in the two categories shows that the proportion of both proximal and distal TEs that are expressed while their closest gene is silent ($TE^{+}gene^{-}$) is higher in the neoplastic cells (39%) signature as compared with the immune cells (24%) signature (Figure 1H). These results show that higher proportions of TEs differentially expressed in neoplastic cells are distant and transcribed independently of their closest gene neighbor, suggesting a higher level of autonomy in TE transcription in GBM tumoral cells.

Tumor enrichment and patient recurrence of the single-cell neoplastic TE signature

To validate the single-cell-based neoplastic TE signature, we next analyzed bulk RNA-seq from the Cancer Genome Atlas (TCGA) (155 GBM patients) and Genotype-Tissue Expression (GTEx) (1,080 healthy samples from 25 tissues; Figures S3A and S3B) cohorts. As previously observed within the single-cell RNA-seq data, the proportion of intronic TEs is higher in normal tissue than in GBM: 53.7% versus 68.6% (Figure S2F). These results indicate that neoplastic GBM cells express higher proportions of non-intronic TEs than non-neoplastic cells and that this difference is detected in both bulk and scRNA-seq datasets.

We next performed principal-component analysis (PCA) and uniform manifold approximation and projection (UMAP) based on neoplastic TE signature, and we show that GBM samples cluster away from normal tissue GTEx samples (Figures 2A, 2B, S3C, and S3D). Heatmap *Z* score representation in TCGA and GTEx samples show higher expression of the 2,000 top TEs from the single-cell neoplastic TE signature in TCGA GBM samples and reduced expression in healthy tissues (Figure 2C). Gene set enrichment analysis (GSEA) shows that expression of the neoplastic TE signature is highly enriched in GBM versus

CellPress
OPEN ACCESS

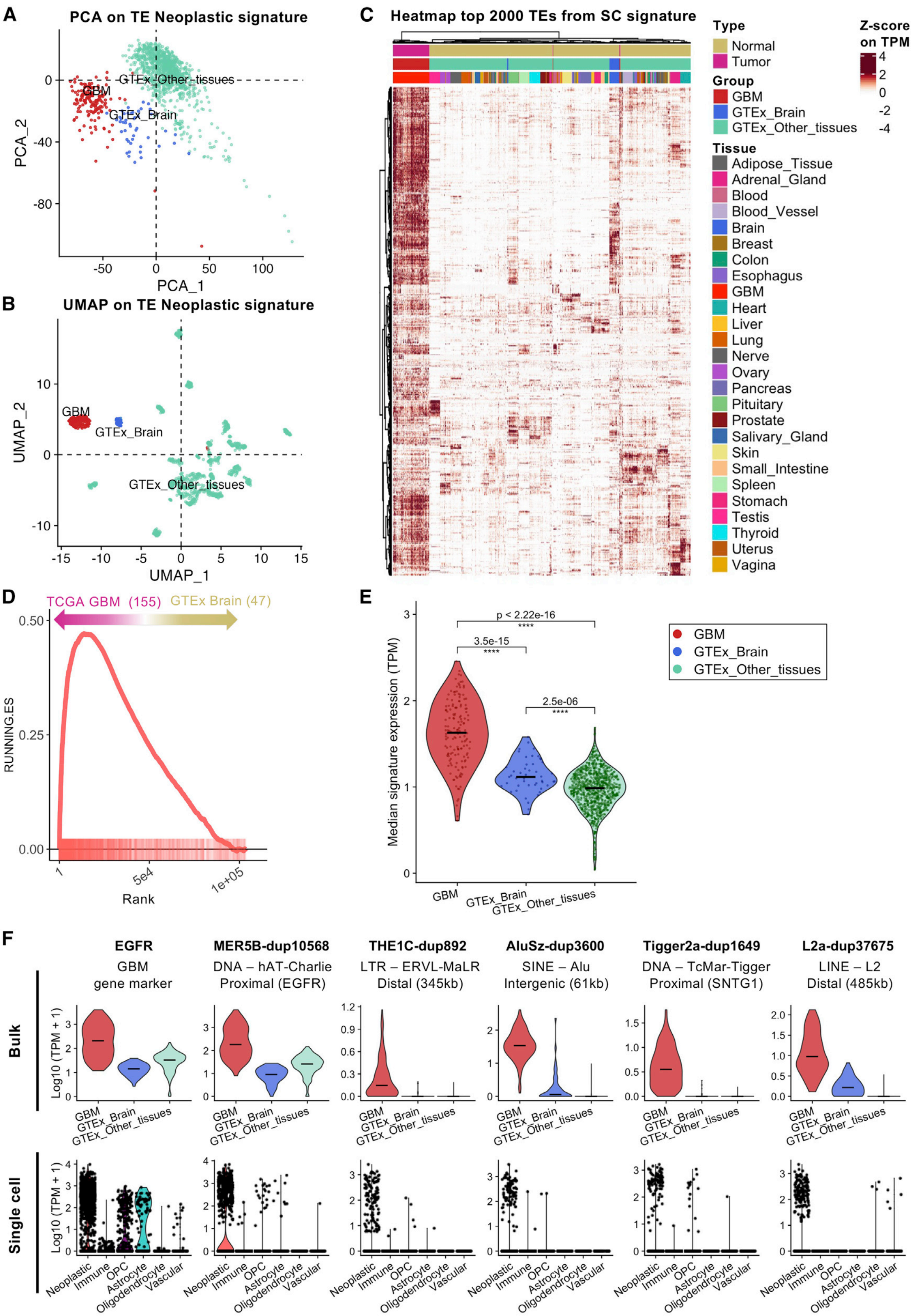

(legend on next page)

normal brain samples (normalized enrichment score [NES] = 1.67 and false discovery rate [FDR] < 0.05; Figure 2D) and versus other normal tissues samples in GTEx (Figures S3E and S3F). The median neoplastic TE signature expression level is also higher in GBM samples, compared with normal-tissue GTEx samples (Figures 2E and S3G). Examples of individual TEs overexpressed in both datasets, bulk RNA-seq (Figure 2F, top panels) and scRNA-seq (bottom panels), illustrate the selective expression of certain TEs in GBM cells as compared with epidermal growth factor receptor (EGFR), a known GBM marker. We conclude that analysis of individual TEs from scRNA-seq is accurate and allows the identification of recurrent, tumor-enriched individual TEs.

TE-derived peptides are presented on HLA-I and are immunogenic *in vitro*

To investigate whether TE-derived peptides are presented by HLA-I molecules in GBM cells, we used 30 mass spectrometry (MS)-based immunopeptidomic samples from GBM primary tumors and cell lines (Forlani et al., 2021; Sarkizova et al., 2020; Shraibman et al., 2016, 2018; Figure 3A). Multi-mapping (3,428) or uniquely mapping (1,945) differentially expressed TEs from the neoplastic TE signature were *in silico* translated in the six reading frames (RFs) and concatenated to the human annotated proteome. We thus obtained 370 TE-derived peptides, including 63 peptides identified in both signatures, 147 only in the multi-mapped reads signature, and 160 only in the uniquely mapped reads signature (Figures 3B and 3C; Data S1). Heatmap representation of all identified TE-derived peptides shows that the number of peptides varies among samples and that some peptides are found in several patients and cell lines (Figure 3D).

TE-derived peptides showed similar SEQUEST quality scores and peptide length distribution as Uniprot-annotated peptides (Figures 3E and S4A). TE-derived peptides binding to HLA-A3 (the most abundant HLA-I among all TE-derived peptides; n = 96) contained the expected binding motif obtained from the Immune Epitope Database (IEDB) (Figure 3F; Vita et al., 2019). In addition, TE-derived peptides maintained the correlation between hydrophobicity and retention time (three representative examples in Figure S4B). These results indicate that TE-derived peptidome is reliable and contains similar characteristics to the canonical peptidome. In addition, 23 TE-derived peptides were synthesized and validated by comparison with the endogenous MS/MS spectra (out of 24 tested; Data S1 and S2). Confirming the robustness of our pipeline, the identified peptides, similar to the neoplastic TE signature, are preferentially encoded by TEs from chromosome 7 and depleted from TEs on chromosome 10 (Figure 3G). We conclude that HLA-I molecules on GBM neoplastic cells present peptides encoded by differentially expressed TEs.

To investigate the possibility that TE-encoded peptides can represent potential tumor antigens, we searched for T cell precursors in healthy donors. Using a tetramer-formation assay, we first experimentally tested the binding for HLA-A*02:01 (six peptides from immunopeptidomics and 17 from NetMHC predictions on *in silico* translated TEs from the neoplastic signature; Figure S4C) and for HLA-B*07:02 (two peptides from the immunopeptidomics) (Figure S4D; Data S1). Nineteen peptides were confirmed as HLA-I binders and were used to test immunogenicity *in vitro*. Peptide-loaded, monocyte-derived dendritic cells were cultured with autologous $CD4^+$ and $CD8^+$ T cells from seven healthy donors, and tetramer staining was used as readout (Figures 3H and S4E). Figure 3H shows examples of expanded populations of TE-specific, tetramer-positive, $CD8^+$ T cells. Mutated Melan-A peptide, a strong binder to HLA-A*02:01 and with high T cell precursor frequency in most healthy donors (Pittet et al., 1999), was used as positive control for cell expansions. Three HLA-A*02:01-binding peptides from canonical proteins not specifically expressed in GBM were also included as negative controls. The three peptides derived from canonical proteins induced very weak or no responses, although mutated Melan-A-derived peptide (also a non-TE-derived, non-GBM-specific protein) induced high T cell responses (Figures 3I and S4F). Expanded tetramer-positive populations were observed for 15 TE-derived peptides (including five from the immunopeptidomic identifications), in at least one donor. These results demonstrate that a subgroup of TEs differentially expressed in GBM can encode HLA-I-binding peptides that are immunogenic *in vitro* in healthy donors and could potentially represent a source of tumor antigens.

Young L1, LTR, and SVA subfamilies are main source of TE-derived HLA-I peptides

To investigate the nature of the neoplastic-enriched TEs that encode HLA-I-presented peptides in GBM, we next mapped the peptide sequences to all differentially expressed TEs from the single-cell neoplastic TE signature. In doing so, we realized that, although 85.4% of the 370 peptides are encoded by one single TE per peptide, the remaining 15% of peptides could potentially be encoded by 2–200 neoplastic differentially expressed TEs per peptide (Figure 4A). We will refer to these peptides as "single-TE" or "multi-TE" encoded peptides, respectively. Several TEs coding for the same peptide will be referred to as "redundant." For further analyses, regarding redundant TEs, since we cannot determine which TE or TEs encodes the peptide, we considered either all the TEs bearing the peptide-coding nucleotide sequence ("all assignments") or

Figure 2. Single-cell neoplastic TE signature is highly enriched in TCGA GBM samples compared with GTEx normal tissues

(A and B) PCA and UMAP projection of TCGA. GBM tumor samples and healthy tissue samples from GTEx based on single-cell neoplastic TE signature are shown.

(C) Heatmap and hierarchical clustering on TCGA GBM tumor and GTEx normal samples representing *Z* score of top 2,000 TEs from the neoplastic TE signature.

(D) GSEA was performed to assess the specific enrichment of the neoplastic TE signature in TCGA GBM tumor samples compared with GTEx normal brain samples.

(E) Violin plot showing the median expression of single-cell neoplastic TE signature in TCGA GBM and GTEx samples (brain and other tissues). We performed unpaired Wilcoxon test: ****p ≤ 0.0001.

(F) Violin plots showing specific expression of EGFR gene and five individual TEs in bulk and single-cell datasets.

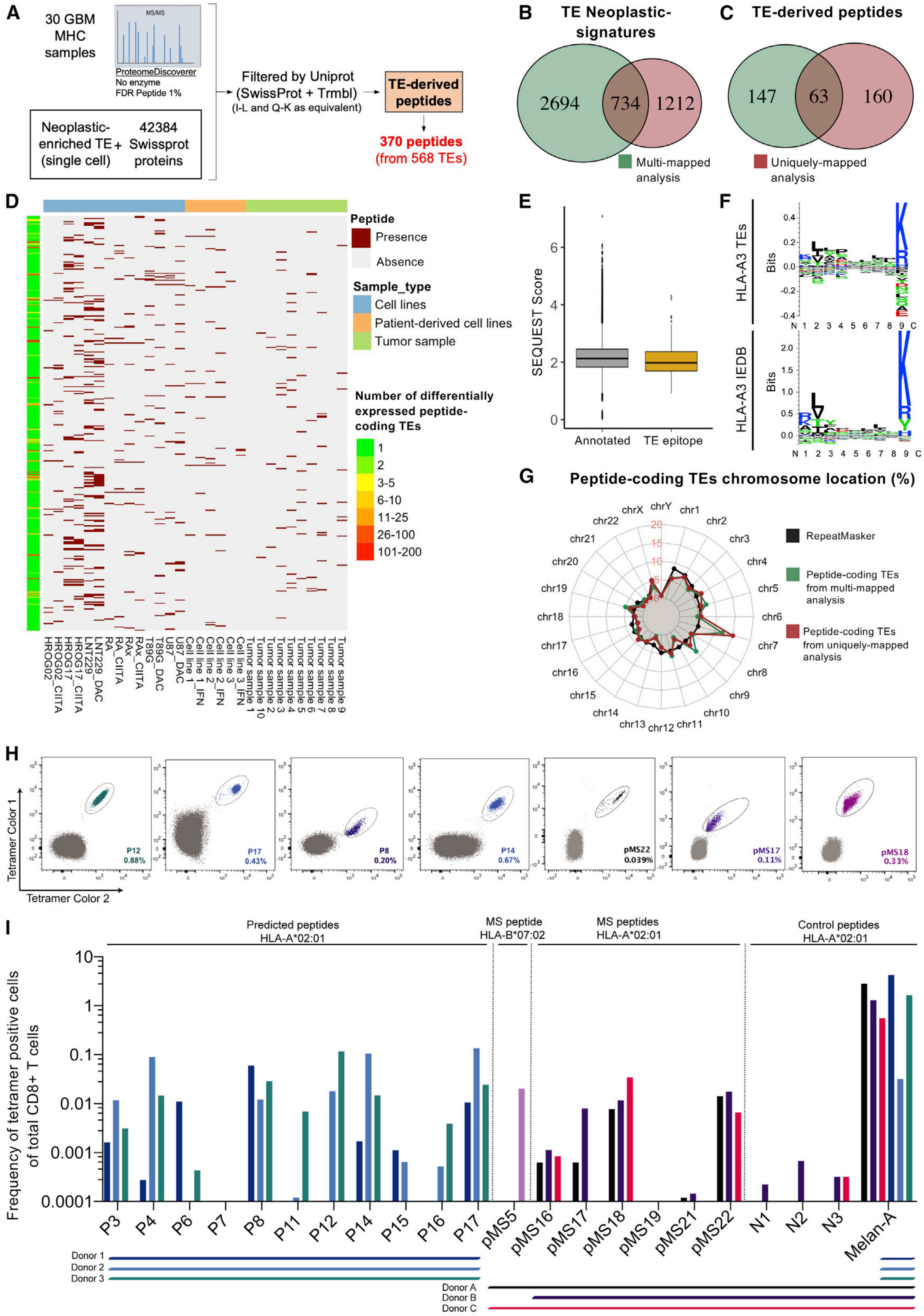

(legend on next page)

only one (chosen uniformly) of these TEs per peptide (‘‘single assignment’’).

We first analyzed the genomic location of the peptide-coding TEs relative to the nearest gene

Among TEs coding for HLA-I-presented peptides, 37.9% and 31.9% (for all and single assignments, respectively) are distal compared with all expressed TEs (12.1%) or to neoplastic differentially expressed TEs (22.3%) (Figure 4B). Analysis of the genomic locations of peptide-coding TEs revealed increased proportions of intergenic TEs (35% and 28.9% for all and single assignments, respectively, compared with 15.2% in the neoplastic TE signature) (Figure 4C). The proportion of intronic TEs is also increased, but not as much (50% and 50.7% for all and single assignments, respectively, compared with 38.7% in TEs expressed in neoplastic cells). 3′ UTR encoded TEs are less frequent in peptide-coding TEs: 25.3% of TEs in the neoplastic TE signature and only 5.8% and 7% for all and single assignments, respectively, among peptide-coding TEs. These results establish selectivity in the genomic location of peptide-coding TEs, which are preferentially distal, intergenic, and not present in 3′ UTRs.

We next sought to investigate whether the identified peptides are preferentially derived from certain TE classes. Based on both all and single assignments, peptide-coding TEs are significantly enriched for LINEs, which represent around 30% of all expressed or neoplastic differentially expressed TEs, and from 52% to 64% for all and single assignments of peptide-coding TEs, respectively (Figure 4D, statistics in Figure S5A, and individually for each immunopeptidomic sample in Figure S5B). These TE class analyses also revealed that TEs classified as ‘‘other’’ are also enriched. This category includes SVA elements and other types of repeats codified in RepeatMasker as RC, RNA, satellite, and unknown. Among the 51 TE-derived peptides in the other category, 23 are from SVA elements (Figure S5C). SINEs, in contrast, are depleted among peptide-coding TEs (from 51.7% to 44.5% in all expressed TEs and neoplastic differentially expressed TEs to around 11% in peptide-coding TEs). Therefore, neoplastic differentially expressed LINEs are a major source of TE-derived peptides presented on HLA-I in GBM.

TEs within each class are classified in families and subfamilies. The evolutionary ‘‘age’’ of these subfamilies can be estimated from the degeneration of their characteristic repeat motifs (Choudhary et al., 2020). We reasoned that the peptides that can be redundantly encoded by multiple TEs could be derived from conserved sequences present in different young TEs from the same subfamilies. Figure 4E shows the age of all TEs from each class in RepeatMasker, as well as all expressed TEs, neoplastic differentially expressed TEs, and peptide-coding TEs. The median age of the peptide-coding SINE and DNA TEs are similar to all genomic TEs annotated in RepeatMasker and to all expressed and neoplastic TE signatures. For LTRs, the proportion of younger TEs is increased among peptide-coding TEs (decreasing the median age of the peptide-coding TEs compared with other categories), but older TEs are also presented on HLA-I. For LINE and other (see above for a more detailed analysis of this category) classes, a bimodal distribution is observed, with a clear enrichment in peptides encoded by TEs from young subfamilies (under 50 Ma) that are rare in RepeatMasker in all expressed and in neoplastic differentially expressed TEs (Figure 4E). We conclude that, among LINE and LTR classes, recent TEs are more prone to provide peptides for HLA-I presentation.

Conserved viral proteins are a source of HLA-I-presented peptides

A few of the youngest subfamilies include TEs that contain intact viral protein ORFs, including a few ‘‘active’’ TEs in terms of retrotransposition (Burns, 2017; Rodic et al., 2015; Scott et al., 2016). We next investigated whether peptides from TEs are derived from validated endogenous viral elements (EVEs) in the gEVE database (Nakagawa and Takahashi, 2016). These EVEs of at least 80 amino acids were identified processing both RepeatMasker annotations and conserved known motifs from viral proteins, such as Gag and Pol. Mapping peptide-coding TEs to gEVE shows that, for both LINEs and LTRs, TEs with an annotated EVE are significantly enriched among peptide-coding TEs (based on both all and single assignments), as compared with RepeatMasker, all expressed, and the neoplastic TE signature (Figure 4F). Consistent with these results, mapping of the TE-derived peptides to annotated EVE protein sequences shows selectivity for Alu among SINEs; L1PA/B/x and L2 among LINEs; ERV1, ERVK, ERVL, and ERV-MaLR among LTRs; and SVA among other (Figure S5C). Allowing one or two nucleotide mismatches (to take into account possible mutations or polymorphisms) increases markedly the proportion of TE-derived peptides that map to annotated EVE protein sequences, including for classes and families (Figure S5C, middle and right panels), suggesting that recently mutated TEs are also a major source of peptides for HLA-I presentation. Most peptides are derived from ORFs bearing a start codon, either ATG (canonical) or CTG/GTG/TTG (non-canonical) (Figures 4G and S5D). We conclude that TEs from young subfamilies, preferentially bearing retroviral protein motifs, are more prone to provide peptides for

Figure 3. GBM-enriched, TE-derived, immunogenic peptides are presented on HLA-I molecules

(A) Workflow for the identification of TE-derived peptides using MS-based immunopeptidomics.

(B and C) Venn diagrams summarizing the overlap between neoplastic TE signatures or TE-derived peptides obtained from uniquely or multi-mapped analysis.

(D) Heatmap summarizing TE-derived peptides found in each immunopeptidomic sample analyzed.

(E) Boxplot showing the peptide-spectrum identification score (SEQUEST score) from annotated-canonical and TE-derived peptides.

(F) HLA-A3 binding motif obtained by GibbsCluster 2.0 from TE-derived peptidome (top) and IEDB reference peptides (bottom).

(G) Radar plot showing the percentage of peptide-coding TEs among all chromosomes.

(H) Examples of expanded tetramer-positive CD8 T cells for TE-derived peptides after *in vitro* immunogenicity assay.

(I) Total frequency of tetramer-positive populations for HLA-A*02:01 predicted or MS-derived peptides and HLA-B*07:02 MS-derived peptides in each evaluated donor. Lines below indicate peptide mixes used for each donor (n = 7). P#, predicted TE-derived peptides; pMS#, MS-derived peptides; mutated Melan-A peptide and N#, normal proteome-derived peptides.

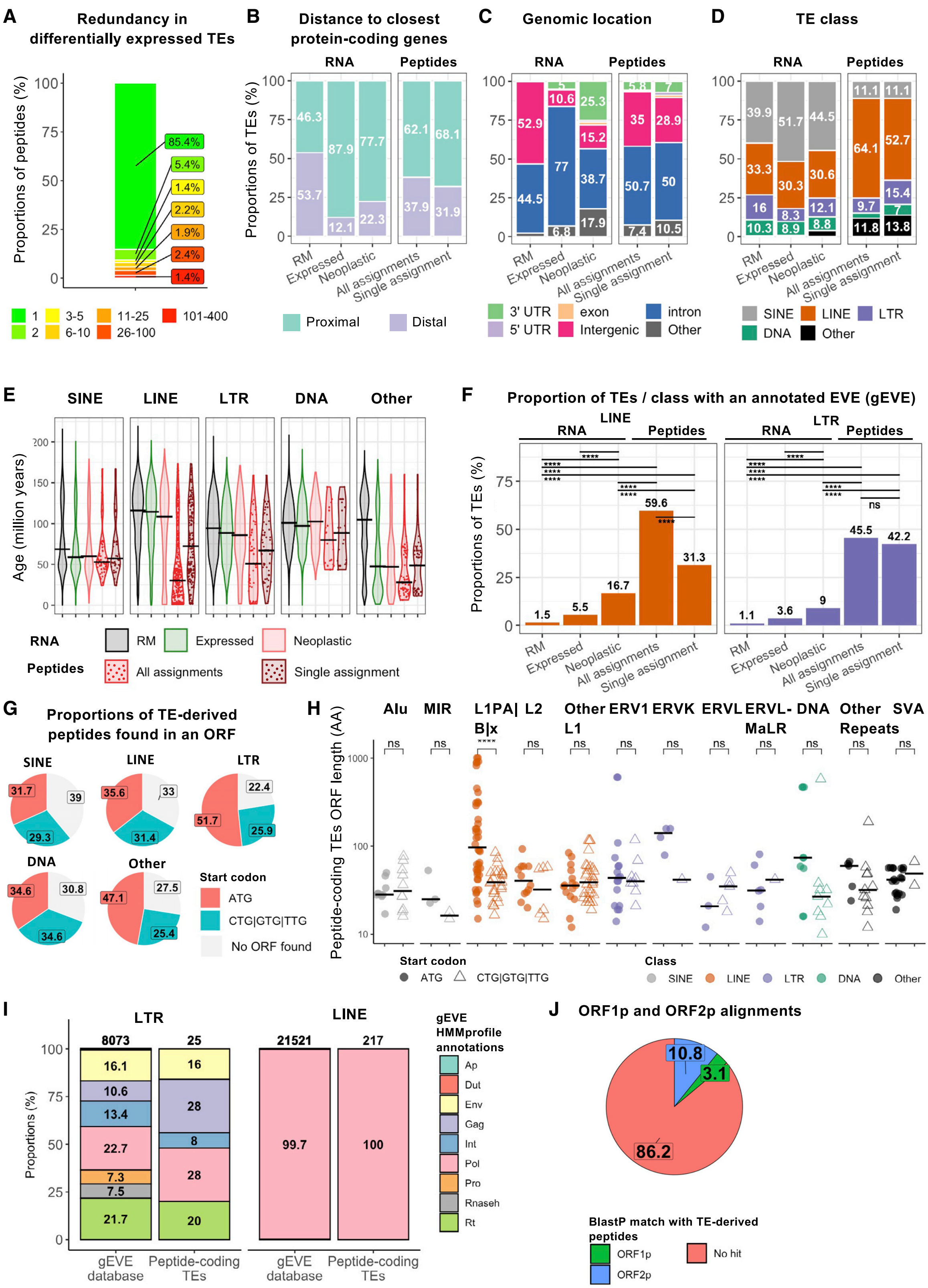

(legend on next page)

presentation on HLA-I molecules in GBM cells. Figure S5E shows an example of three peptides encoded by an SVA family member, SVA_B_dup189. Peptides can be encoded by different reading frames (RFs) and rarely outside of ORFs. In these cases, it could be that the ORF is shorter than 30 nt, that the start codon for this ORF is not among the four start codons used in the pipeline, or that the start codon is upstream the TE sequence.

Analysis of the length of the ORFs encoding HLA-I-presented peptides shows that, among L1PA/B/x, but not among other TE families, ORFs generating peptides and containing a canonical ATG start codon are longer than the ORFs beginning with a non-canonical start codon (Figure 4H). Among peptide-coding LTRs mapping to a gEVE annotated ORF, ORFs from all retroviral proteins are found in the peptide-coding TE sequences (Figure 4I), with an enrichment for Gag (which represents 10.6% of LTR EVE annotated versus 28% of LTR peptide-coding TEs). In the case of LINEs, Pol are the only gEVE-annotated proteins (Figure 4I). Blast of the peptide-coding sequences shows that the majority of LINE-encoded peptides are not derived from the two major LINE ORFs, ORF1p (3.1%) and ORF2p (10.8%) (Figure 4J). Therefore, TE-derived peptides are derived from 10- to 1,000-amino-acids-long ORFs bearing canonical or alternative start codons.

TE subfamilies share HLA-I-presented peptide coding sequences

To investigate whether some types of TEs are more prone to provide HLA-I-binding peptides than others, we next compared the proportions of TE families among the ones differentially expressed in GBM (and used for the immunopeptidomic search) and the proportions found among the TEs that code for peptides. Figure S6A shows that, for LTRs, SINEs, and other, the proportions of most families are similar between the neoplastic TE signature and peptide-coding TEs (both with all or single assignments) (Figure S6A, middle and right panels). For LINEs, in contrast, peptides are preferentially derived from L1PA/B/x: 25.3% in the neoplastic TE signature versus 76.6% or 49.7% for all and single assignments, respectively. Other LINE families are depleted among peptide-coding TEs (especially L2, which represents 25.1% of LINE in the neoplastic TE signature and provides for only 7.4% or 15.4% of LINE peptide-coding TEs, with all and main assignments, respectively) (Figure S6A, left panel). Statistical analysis shows significant enrichment in peptide-coding TEs over neoplastic differentially expressed TEs for L1PA/B/x and SVA, considering either all or single assignments (Figures 5A and S6B). ERV1 and "other L1" are enriched with all assignments, while on the other hand, ERVKs are enriched with single assignment. "Other repeats," classified in RepeatMasker as RC, RNA, satellite, and unknown, are also enriched. L2, SINEs (including Alu and MIR), and ERVs (including ERVL and ERVL-MalR) are all significantly depleted among peptide-coding TEs, as compared with neoplastic differentially expressed TEs (Figures 5A and S6B). L1PA/B/x includes L1HS (or L1PA1, TE subfamily with few members still active in human genome) and their closely related subfamilies L1PA(x) and L1PB(x), which are all among the younger subfamilies compared with other LINE-1 subfamilies. We conclude that some recent, mainly LINE-1, TE families preferentially generate HLA-I-presented peptides in GBM.

Because recent TEs have more conserved repeat motifs, we next sought to investigate whether multi-TE-encoded, HLA-presented peptides corresponded to shared subfamily motifs. We represented the 152 TE subfamilies coding for the 370 identified HLA peptides in 2-dimensional plots coloring the intersections between two subfamilies according to the number of shared peptides. The green diagonal in this plot indicates that most subfamilies code for only one peptide (Figure 5B). The three main groups of TE subfamilies coding shared peptides, or "redundancy clusters," appear as large squares and are enlarged in Figure 5B (bottom panel). The first redundancy cluster corresponds to a group of L1HS and L1PA(x), which are young subfamilies of LINE-1 elements that share up to 25 peptides, pairwise. The second cluster identifies relatively young SINEs (mainly Alu) that share single peptides. The third cluster corresponds to a group of young subfamilies of SVA elements that share variable numbers of peptides. Therefore, redundancy occurs within multiple TEs from the same recent related subfamilies that could all potentially code for multiple peptides presented on HLA-I molecules. Redundancy in peptide-coding TEs is therefore limited to a small number of recent TE subfamilies.

To investigate further the links between redundancy and age of TEs, we extended the analysis to all TEs in the genome (redundancy was so far analyzed among the neoplastic TE signature). Genomic TE redundancy analysis shows that 49.5% of the 370 peptides identified by immunopeptidomics are encoded by only one TE in the genome (Figure 5C) (as compared with 85.4% in the neoplastic TE signature; Figure 4A). At the opposite end, 15.9% of these peptides could potentially be encoded by 201–13,500 TE occurrences in the genome. A plot of each peptide according to the number of TEs it can potentially be encoded by and the age of the corresponding subfamilies is shown in Figure 5D. Among SINEs, Alu-derived peptides are highly redundant and from recent subfamilies, while the MIR-derived peptides are encoded by

Figure 4. TE-derived peptides are located in long ORFs starting with canonical and non-canonical start codons

(A) Barplot showing the proportion of peptides encoded by one or several TEs from the single-cell neoplastic signature.

(B–D) Bar plots displaying proportions of proximal and distal TEs (B), genomic location proportions (C), and TE class proportions (D) at RNA and peptide levels.

(E) Violin plots representing the TE age distribution per class and subset.

(F) Bar plots showing for different subsets the quantification of LINE and LTR TEs with an endogenous viral element ORF documented in gEVE database. We performed proportion test. ns: $p > 0.05$; *$p \leq 0.05$; **$p \leq 0.01$; ***$p \leq 0.001$; ****$p \leq 0.0001$.

(G) Pie charts showing the percentage of TE-derived peptides found in an ORF with a canonical or non-canonical start codon.

(H) Plot showing the peptide-coding TE ORF length distribution depending on the type of start codon. We performed unpaired wilcoxon test. ns: $p > 0.05$; *$p \leq 0.05$; **$p \leq 0.01$; ***$p \leq 0.001$; ****$p \leq 0.0001$.

(I) Bar plots displaying the proportions of LTRs and LINEs matching a hidden Markov model (HMM) profile of a known viral protein motif in gEVE.

(J) Pie chart representing the percentage of LINE-derived peptides matching ORF1p and ORF2p proteins (from Uniprot) using BlastP alignment.

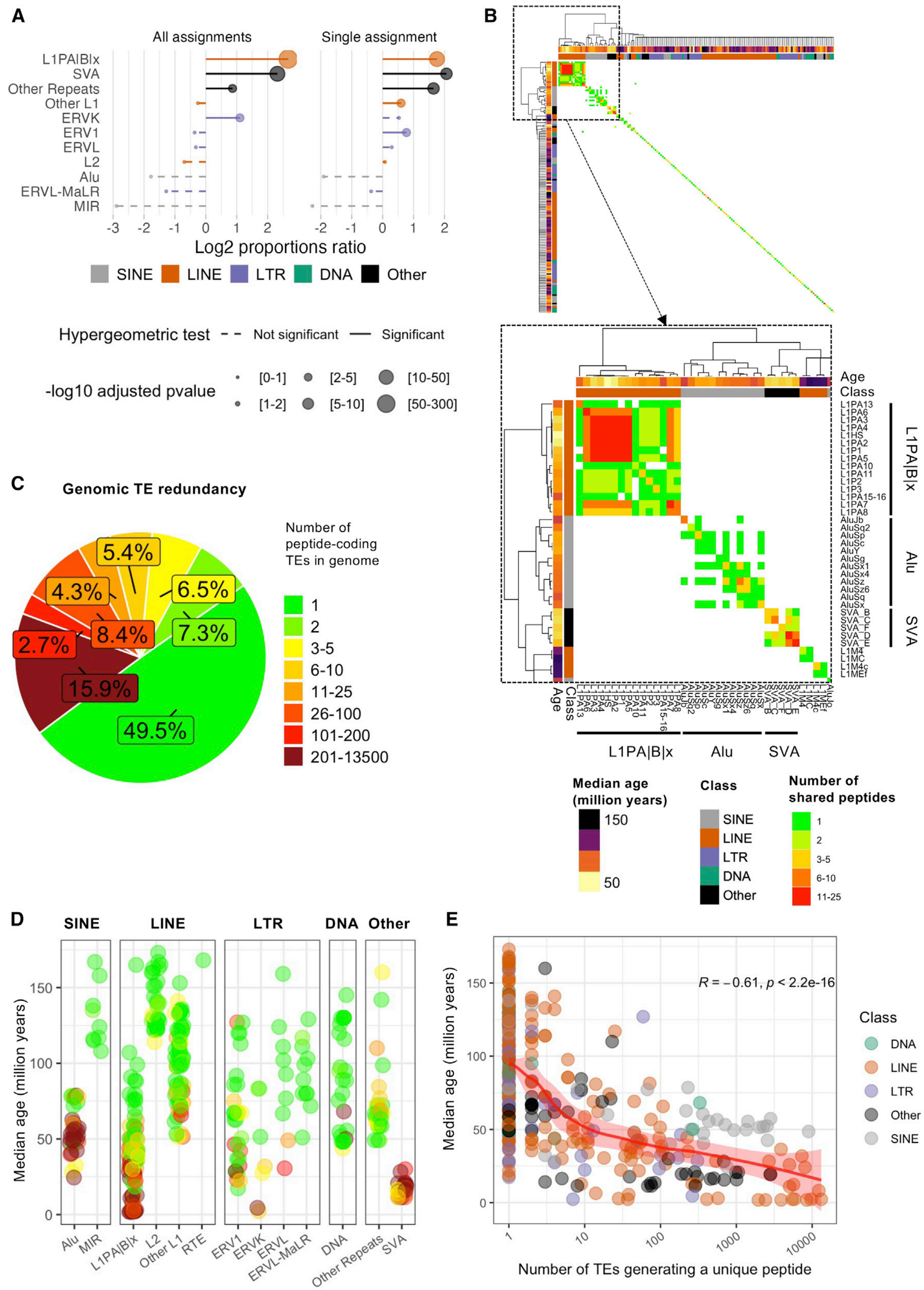

(legend on next page)

single TEs from older subfamilies. The same correlation is observed among LINE-1 peptides, with young L1HS-, L1PA(x)-, and L1PB(x)-derived peptides being encoded by multiple elements and peptides derived from older L2 and "other L1" subfamilies by single elements. The negative correlation between the number of TEs potentially encoding single peptides and the age of the corresponding TE subfamilies is confirmed across all TE families ($r = -0.61$; Figure 5E). We conclude that, regardless of TE classes (LINE, SINE, LTR, or DNA), subfamilies of young TEs bear shared (redundant) sequences that could code for the same HLA-I peptide, while peptides encoded by TEs from older, more degenerated subfamilies are vastly derived from one genomic sequence.

Ancient single-TE encoded peptides are more tumor enriched

To investigate how redundancy of TE-derived peptides affects tumor specificity, we next calculated for each TE-derived peptide the ratio between the aggregate expression of all TEs coding for the same peptide in TCGA GBM versus all healthy tissues from GTEx samples (Figure 6A; brown for higher expression in GBM and blue for the opposite). Unsupervised clustering of the aggregate TE expression identifies two main groups of TE-derived peptides, group 1 and 2, dominated by peptide-coding TEs overexpressed in GTEx and in GBM, respectively. Group 1 contains higher proportions of LINEs and others (including all 23 peptide-coding SVA elements), while group 2 contains more LTRs and DNA transposons (Figure 6A, right panels). Moreover, group 1 contains a majority of multi-TE encoded peptides (63.5%), compared with only 26.6% in group 2 (Figure 6A). Consistently, the median age of group 1 TEs is significantly lower than the median age of group 2 (Figure 6B). These results show that single-TE encoded peptides from older TE subfamilies are more likely to be overexpressed in GBM than TEs from younger subfamilies containing multi-TE encoded peptides.

Can we, then, identify tumor-specific TE peptides? Figure 6C shows expression of the top 50 tumor-enriched, peptide-coding TEs in GBM and all GTEx healthy tissues (as 90 percentile expression, left panel, and percentage of samples with higher expression than GBM median expression, right panel). The most tumor-enriched TEs are from diverse classes but are preferentially derived from ORFs containing a canonical start codon (right histograms in Figures 6C and S7A). Some of these TEs are expressed in a majority of GBM tumors and undetectable in all, or in a majority, of GTEx healthy tissues (including brain) (Figure 6D). For some of these TEs, over 90% of the cells expressing the TEs are GBM neoplastic cells from all four patients in the scRNA-seq datasets (pie charts in Figure 6D; violin plots in Figure S7B). We conclude that a subset of non-redundant, peptide-coding TEs are highly tumor enriched and recurrent in cancer patients. These non-redundant, peptide-coding TEs represent interesting potential targets for immunotherapy.

DISCUSSION

In search for tumor-specific, recurrent antigens, we use a TE-centered proteogenomic approach to investigate HLA-I presentation of TE-derived peptides. We first analyze scRNA-seq from total live cells of four primary GBM tumors to identify individual TEs expressed selectively in GBM tumor cells and not in hematopoietic or stromal cells. We show that the TEs differentially expressed in neoplastic cells are overexpressed in a cohort of 155 bulk RNA-seq samples from GBM patients (TCGA), as compared with all tissues, including brain tissue from healthy donors (GTEx). This neoplastic-enriched TE signature is used to interrogate MS-based immunopeptidomic datasets from 30 cell lines and primary GBM tumors. We identify 370 TE-derived peptides with reliable profiles and motif compliance to HLA-I alleles of the corresponding samples. These peptides are encoded by 568 TEs, whose analysis revealed some interesting aspects of the biology of HLA-I presentation of peptides from TEs in GBM cells.

Our study relies on scRNA-seq mapping of TEs. Several recent papers have analyzed TEs in scRNA-seq datasets. Although a few early studies pointed to possible bias and limitations (He et al., 2021; Shao and Wang, 2021), reliable pipelines and guidelines are now available and have been applied in our study. Our results are also supported by internal controls that confirm the robustness of our TE scRNA-seq analyses. First, we show that the TEs expressed in neoplastic GBM cells, but not in other cell populations, are biased for TEs encoded by chromosome 7 (all or intergenic TEs, suggesting that the bias is not due to intronic TE expression) (Figure 1E). Second, the neoplastic TE signature based on scRNA-seq is overexpressed in GBM bulk RNA-seq patient cohorts compared with healthy tissues (Figures 2D and 2E). Importantly, the peptides identified in immunopeptidomic databases are also biased for chromosome 7, further and independently validating our peptide discovery and validation pipelines.

One conclusion of our study is that the proportions of intronic and intergenic TEs are increased among peptide-coding TEs, as compared with the neoplastic TE signature (the database used to identify the peptides), at the expense of 3′ UTR TEs. HLA-I-presented peptides can therefore be derived from both gene-dependent and gene-independent transcription and translation, but the reasons why intronic TEs provide proportionally more peptides than 3′ UTR TEs is worth further analyses. Previous studies have found that 3′ UTRs can code for HLA-presented peptides (Laumont et al., 2016; Zhao et al., 2020), but these

Figure 5. TE-derived peptide redundancy depends on the age of TEs

(A) Plot showing TE family enrichment analysis using peptide-coding TEs with all or single assignment(s).

(B) Plot showing the number of shared TE-derived peptides among TE subfamilies. A closed-up representation is displayed on the bottom, showing the number of shared peptides between L1PA/B/x, SVA, and Alu subfamilies.

(C) Pie charts displaying the percentage of redundancy of TE-derived peptides.

(D) Dot plot representing the median age of peptide-coding TEs in each family classified by TE classes.

(E) Correlation plot between the total number of peptide-coding TEs and their median age. We performed Pearson correlation test. Pearson coefficient and p value are indicated on the figure.

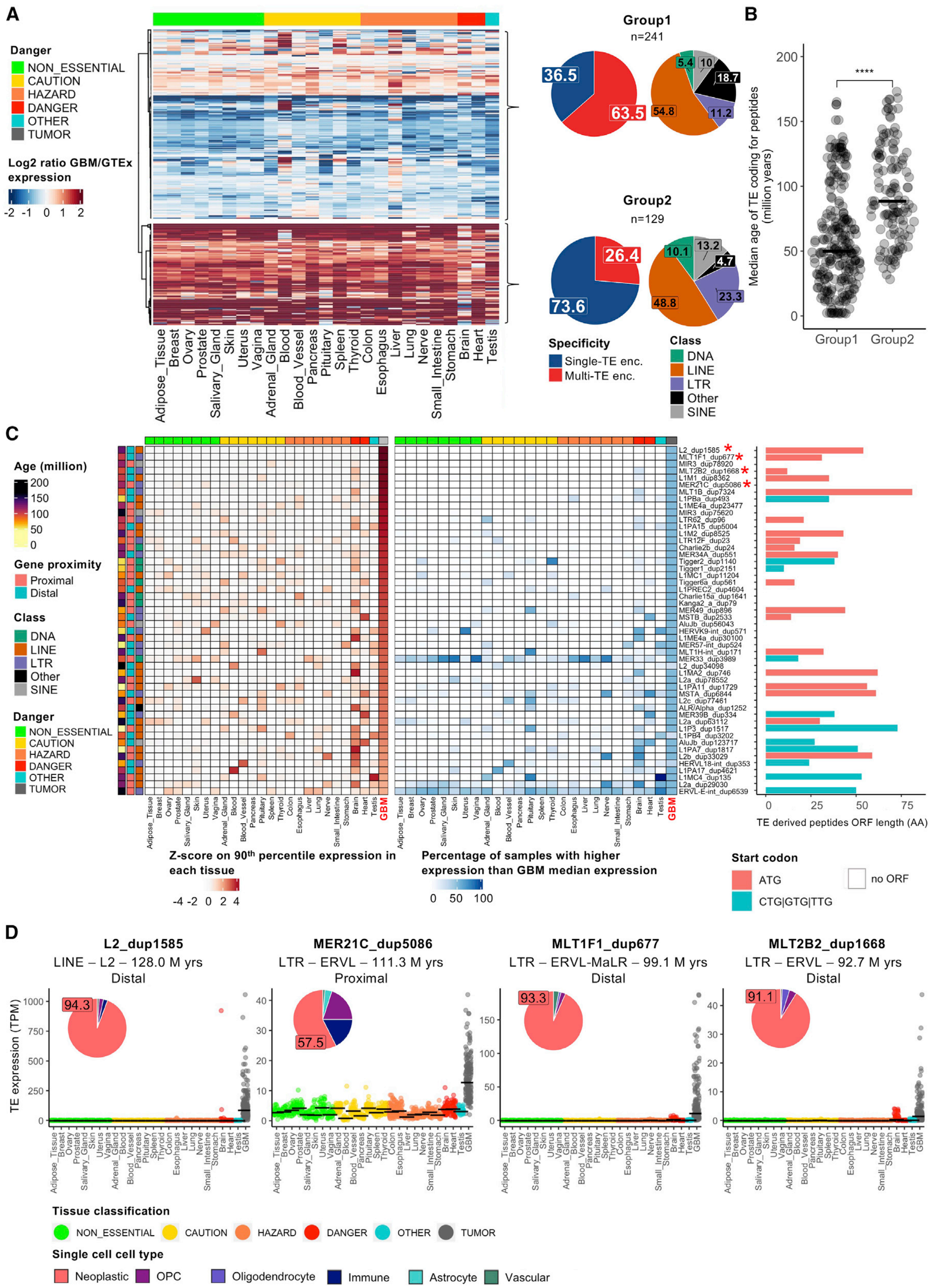

(legend on next page)

studies did not consider TEs from other genomic locations, as we do here. We also find that LINE-1 elements are the major source of HLA-I-presented peptides in GBM. LINE-1 represents around 30% of TEs in the human genome, of all TEs expressed in GBM, and of neoplastic TE signature but over 50% of the TE-encoded peptides presented on HLA-I. SVA-derived peptides are also strongly enriched, while the proportion of SINE-derived peptides is reduced (as compared with genomic, expressed, and differentially expressed SINEs in GBM). LINE-1 elements with and without intact ORFs are preferentially represented among peptide-generating TEs, and this bias is observed whether TEs are assigned to multiple or to single locations, indicating that the bias is not due to TE mapping issues.

Another conclusion from our study is that HLA-I molecules present peptides that can be encoded by either one or multiple TEs (bearing nucleotide sequence encoding the exact same peptide). Redundancy, in most cases, occurs within TE subfamilies and, in some cases, within different subfamilies that are always from the same TE class. The most redundant TEs (from several hundred to several thousand occurrences) are from L1PA/B/x and often bear intact annotated ORFs. Peptides derived from Alu (a SINE family member), ERV1 (an LTR family), and SVA (an intermediate-length independent family), which are all among the youngest TE families in humans, are also highly represented and redundant. Redundancy is negatively correlated with the age of the TE subfamily, suggesting that the recurrent sequences encoding HLA-I-binding peptides are part of the ancestral TE insertion event, which subsequently degenerated by mutations and disappeared with time as members of the subfamilies diverged. This scenario is supported by the observation that, if one or two nucleotide mismatches are allowed, the number of redundant TEs is even larger (Figure S5C). This is an intriguing observation, and we do not know yet whether the peptides identified by mass spectrometry are derived from multiple or single TE loci.

Analysis of the peptide-coding TE ORFs reveals that peptides are generally encoded by 10- to 100-amino-acid-long ORFs (with the exception of around half of the LINE-encoded peptides that are derived from longer ORFs). In LTRs, peptides are derived from all viral ORF types, with a positive bias for gag-derived peptides, as compared with the proportion of gag genes annotated in the databases (Figure 4I). Among LINE-derived peptides, only a small proportion (around 10%) are derived from the known ORF1p and ORF2p proteins. The TE-coding ORFs bear either canonical or alternative start codons, with exception of the longer LINE-1 ORFs (over 100 amino acids), which are all driven by canonical ATG start codons.

How, then, can we use this knowledge to identify tumor-specific, TE-derived antigens? Analysis of the relative expression of individual peptide-coding TEs in GBM tumors and a wide series of healthy tissues reveal that redundant TEs from younger subfamilies are generally less tumor enriched than single TEs from older ones (Figure 6A). Because of their wide tissue expression, it is most likely that the immune system is more tolerized to the antigens from these TEs (although this would need to be addressed specifically). Redundant TEs are therefore probably not the best candidates for tumor-specific targets for immunotherapy, although vaccination with LINE-1 intact ORFs has been shown to be both immunogenic and safe in mice and monkeys (Sacha et al., 2012). Our results, however, also identify non-redundant, peptide-coding TEs that are preferentially from MIR, LINE-1 and -2, and some ERV oldest subfamilies. These non-redundant, peptide-coding TEs are in majority from relatively old TE subfamilies (over 50 Ma), and tBLASTn analysis shows that some of these sequences are present only once in the genome. Some of these TEs are from subfamilies recurrently and selectively de-repressed in tumors, mostly through local DNA demethylation (Brocks et al., 2017; Chiappinelli et al., 2017; Lavie et al., 2005; Ohtani et al., 2020; Roulois et al., 2015; Sacha et al., 2012). We show that some of these peptide-coding TEs that are expressed in a majority of GBM tumors are either not detected in healthy tissues or detected at low frequencies and/or low levels (Figure 6). Further studies will investigate whether these tumor-enriched, peptide-coding TEs can be expressed in other pathological conditions, such as apoptosis or inflammation, in which TE de-repression can be observed.

Our results of *in vitro* stimulation with some of the TE-derived peptides indicate that the TCR repertoire for TEs in healthy individuals exists, opening the possibility that these TEs are immunogenic in patients. Previous studies, however, have shown T cell reactivity against tumor-expressed TEs, establishing the proof of concept that TEs, including ERVs, can be immunogenic in cancer patients (Saini et al., 2020; Smith et al., 2018; Wang-Johanning et al., 2008). In this context, mapping the expression of individual TEs from single-cell and bulk RNA-seq in cancer patients proved efficient in defining individual TE occurrences that yield HLA-I-presented peptides. The tumor enrichment and high recurrence of these peptide-coding TEs opens perspectives for immunotherapies in many cancer types with de-repressed TEs and beyond, in other pathologies in which TEs expression is de-regulated.

Limitations of the study

First, our study maps RNA-seq reads to annotated TEs. At least in part because TEs are largely repetitive, TE annotation in the

Figure 6. A subset of non-redundant, peptide-coding TEs are highly tumor enriched and recurrent in cancer patients

(A) Heatmap displaying the log2 ratio between TCGA GBM and GTEx samples of TE-derived peptides aggregate RNA-related expression. GTEx tissues are classified into five normal tissue categories defined in Bradley et al. (2020) (left). Hierarchical clustering identified two groups. Distribution of redundancy and TE classes is shown for each group (right).

(B) Plot showing median age of peptide-coding TEs for each group. We performed unpaired Wilcoxon test. The correspondence between p values and symbols is as follows: ns: $p > 0.05$; *$p \leq 0.05$; **$p \leq 0.01$; ***$p \leq 0.001$; ****$p \leq 0.0001$.

(C) Heatmaps of top 50 TEs from group 2 coding for single-TE encoded peptide displaying their 90^{th} percentile expression (left) and frequency (middle) in GBM tumor samples and 25 normal tissues from GTEx. ORF length is plotted (right) for each TE.

(D) Plots showing TE expression for four examples marked with a star in (C). Median expression for each tissue is indicated with a black line. The percentage of positive cells in each cell type described in scRNA-seq is represented using pie charts.

human genome is far from perfect (even it has made significant progress in the last few years). Consequently, it is possible that the genomic location and the assignment to a specific locus or subfamily will change in the coming years. Second, even if our analysis of T cell stimulation in healthy peripheral blood mononuclear cells (PBMCs) shows potential immunogenicity, the actual direct demonstration of TE immunogenicity would come from analyses of T cell responses in GBM patients. This is not trivial, as tumor-infiltrating lymphocytes (TILs) in GBM are rare and difficult to amplify *ex vivo*. Thirdly, despite our demonstration that numerous transcribed TEs can potentially code for some of the identified HLA-I-bound peptides, we still do not know which and how many of those TEs actually encode the peptides. Finally, even if the expression of some TEs seems truly specific (absent completely from all healthy tissues), these TEs are very rare (maybe three in this study). Tumor-enriched TEs in contrast are quite numerous and could be sufficiently immunogenic to develop effective immunotherapy tools.

STAR★METHODS

Detailed methods are provided in the online version of this paper and include the following:

- KEY RESOURCES TABLE
- RESOURCE AVAILABILITY
  - Lead contact
  - Materials availability
  - Data and code availability
- EXPERIMENTAL MODEL AND SUBJECT DETAILS
  - Human research participants
  - In-vitro vaccinations assay
  - Tetramer staining and analysis
- METHOD DETAILS
  - Transposable element annotations
  - Ancient viral protein motif identification
  - Analysis of known TE proteins
  - Single-cell data analysis
  - Quantification of gene and TE expression
  - Filtering features and cells, normalization and batch correction
  - Dimensionality reduction
  - Differential expression analysis and enrichment tests
  - Radarplot and chromosome distribution
  - Bulk RNA-seq data analysis
  - Downstream analysis of bulk RNA-seq samples
  - Gene set enrichment analysis
  - Mass spectrometry based immunopeptidomics
  - Peptide hydrophobicity index (HI) calculation
  - Single and all assignments definition
  - Identifying potential peptide-coding TEs
  - Spectrum validation with synthetic peptides
  - Assessing related RNA expression of TE-derived peptides
- QUANTIFICATION AND STATISTICAL ANALYSIS
  - Figures
  - Statistical analyses

SUPPLEMENTAL INFORMATION

Supplemental information can be found online at https://doi.org/10.1016/j.celrep.2022.110916.

ACKNOWLEDGMENTS

We thank all the U932 members, Olivier Lantz, Maude Delost, Nathalie Amzallag, and Florence Faure, for helpful discussions. Also, we are grateful to Joshua J. Waterfall for helpful discussion and bioinformatics advice. In addition, we thank the core facilities at Curie Institute, including the Bioinformatics groups. S.A. received funding from the Institut Curie, Institut National de la Santé et de la Recherche Médicale, and Centre National de la Recherche Scientifique. This work has received support under the program « Investissements d'Avenir » launched by the French Government. We thank the Ligue Nationale Contre Le Cancer for the fellowship to Y.A.A.

AUTHOR CONTRIBUTIONS

C.G. and S.A. conceived and designed the project. P.-E.B. and C.G. designed, performed bioinformatics analyses, and interpreted data. A.M. designed, performed *in vitro* vaccination experiments, and analyzed the results. Y.A.A. performed and analyzed proteomics data. M.C. and Y.A.A. carried out experimental work about validation of peptides. J.V.Z. and Z.A.B. contributed to experimental work. C.A., Z.A.B., and E.Z. provided critical revisions to the manuscript. S.A., C.G., P.-E.B., A.M., and Y.A.A. wrote the manuscript and interpreted data.

DECLARATION OF INTERESTS

C.A. is a consultant for Biotherapy Partners. S.A. is shareholder and consultant for Mnemo Therapeutics. P.-E.B., Y.A.A., A.M., E.Z., and C.G. are consultants for Mnemo Therapeutics. A patent related to this work has been deposited under number EP22305355 in European Patent Application.

Received: September 21, 2021
Revised: March 22, 2022
Accepted: May 12, 2022
Published: June 7, 2022

REFERENCES

Almeida, L.G., Sakabe, N.J., deOliveira, A.R., Silva, M.C.C., Mundstein, A.S., Cohen, T., Chen, Y.T., Chua, R., Gurung, S., Gnjatic, S., et al. (2009). CTdatabase: a knowledge-base of high-throughput and curated data on cancer-testis antigens. Nucleic Acids Res. *37*, D816–D819. https://doi.org/10.1093/nar/gkn673.

Andersen, R.S., Kvistborg, P., Frosig, T.M., Pedersen, N.W., Lyngaa, R., Bakker, A.H., Shu, C.J., Straten, P.t., Schumacher, T.N., and Hadrup, S.R. (2012). Parallel detection of antigen-specific T cell responses by combinatorial encoding of MHC multimers. Nat. Protoc. *7*, 891–902. https://doi.org/10.1038/nprot.2012.037.

Anwar, S.L., Wulaningsih, W., and Lehmann, U. (2017). Transposable elements in human cancer: causes and consequences of deregulation. Int. J. Mol. Sci. *18*, 974. https://doi.org/10.3390/ijms18050974.

Boon, T., and van der Bruggen, P. (1996). Human tumor antigens recognized by T lymphocytes. J. Exp. Med. *183*, 725–729. https://doi.org/10.1084/jem.183.3.725.

Bradley, S.D., Talukder, A.H., Lai, I., Davis, R., Alvarez, H., Tiriac, H., Zhang, M., Chiu, Y., Melendez, B., Jackson, K.R., et al. (2020). Vestigial-like 1 is a shared targetable cancer-placenta antigen expressed by pancreatic and basal-like breast cancers. Nat. Commun. *11*, 5332. https://doi.org/10.1038/s41467-020-19141-w.

Brennan, C.W., Verhaak, R.G.W., McKenna, A., Campos, B., Noushmehr, H., Salama, S.R., Zheng, S., Chakravarty, D., Sanborn, J.Z., Berman, S.H., et al.

(2013). The somatic genomic landscape of glioblastoma. Cell *155*, 462–477. https://doi.org/10.1016/j.cell.2013.09.034.

Brocks, D., Schmidt, C.R., Daskalakis, M., Jang, H.S., Shah, N.M., Li, D., Li, J., Zhang, B., Hou, Y., Laudato, S., et al. (2017). DNMT and HDAC inhibitors induce cryptic transcription start sites encoded in long terminal repeats. Nat. Genet. *49*, 1052–1060. https://doi.org/10.1038/ng.3889.

Burns, K.H. (2017). Transposable elements in cancer. Nat. Rev. Cancer *17*, 415–424. https://doi.org/10.1038/nrc.2017.35.

Butler, A., Hoffman, P., Smibert, P., Papalexi, E., and Satija, R. (2018). Integrating single-cell transcriptomic data across different conditions, technologies, and species. Nat. Biotechnol. *36*, 411–420. https://doi.org/10.1038/nbt.4096.

Carreno, B.M., Magrini, V., Becker-Hapak, M., Kaabinejadian, S., Hundal, J., Petti, A.A., Ly, A., Lie, W.R., Hildebrand, W.H., Mardis, E.R., and Linette, G.P. (2015). A dendritic cell vaccine increases the breadth and diversity of melanoma neoantigen-specific T cells. Science *348*, 803–808. https://doi.org/10.1126/science.aaa3828.

Castle, J.C., Kreiter, S., Diekmann, J., Lower, M., van de Roemer, N., de Graaf, J., Selmi, A., Diken, M., Boegel, S., Paret, C., et al. (2012). Exploiting the mutanome for tumor vaccination. Cancer Res. *72*, 1081–1091. https://doi.org/10.1158/0008-5472.can-11-3722.

Chauvin, J.M., Pagliano, O., Fourcade, J., Sun, Z., Wang, H., Sander, C., Kirkwood, J.M., Chen, T.h.T., Maurer, M., Korman, A.J., and Zarour, H.M. (2015). TIGIT and PD-1 impair tumor antigen-specific CD8(+) T cells in melanoma patients. J. Clin. Invest. *125*, 2046–2058. https://doi.org/10.1172/jci80445.

Chiappinelli, K.B., Strissel, P.L., Desrichard, A., Li, H., Henke, C., Akman, B., Hein, A., Rote, N.S., Cope, L.M., Snyder, A., et al. (2017). Inhibiting DNA methylation causes an interferon response in cancer via dsRNA including endogenous retroviruses. Cell *169*, 361. https://doi.org/10.1016/j.cell.2017.03.036.

Chong, C., Muller, M., Pak, H., Harnett, D., Huber, F., Grun, D., Leleu, M., Auger, A., Arnaud, M., Stevenson, B.J., et al. (2020). Integrated proteogenomic deep sequencing and analytics accurately identify non-canonical peptides in tumor immunopeptidomes. Nat. Commun. *11*, 1293. https://doi.org/10.1038/s41467-020-14968-9.

Choudhary, M.N., Friedman, R.Z., Wang, J.T., Jang, H.S., Zhuo, X., and Wang, T. (2020). Co-opted transposons help perpetuate conserved higher-order chromosomal structures. Genome Biol. *21*, 16. https://doi.org/10.1186/s13059-019-1916-8.

Consortium, G.T. (2013). The genotype-tissue expression (GTEx) project. Nat. Genet. *45*, 580–585. https://doi.org/10.1038/ng.2653.

Coulie, P.G., Lehmann, F., Lethe, B., Herman, J., Lurquin, C., Andrawiss, M., and Boon, T. (1995). A mutated intron sequence codes for an antigenic peptide recognized by cytolytic T lymphocytes on a human melanoma. Proc. Natl. Acad. Sci. U S A *92*, 7976–7980. https://doi.org/10.1073/pnas.92.17.7976.

Darmanis, S., Sloan, S.A., Croote, D., Mignardi, M., Chernikova, S., Samghababi, P., Zhang, Y., Neff, N., Kowarsky, M., Caneda, C., et al. (2017). Single-cell RNA-seq analysis of infiltrating neoplastic cells at the migrating front of human glioblastoma. Cell Rep. *21*, 1399–1410. https://doi.org/10.1016/j.celrep.2017.10.030.

Dobin, A., Davis, C.A., Schlesinger, F., Drenkow, J., Zaleski, C., Jha, S., Batut, P., Chaisson, M., and Gingeras, T.R. (2013). STAR: ultrafast universal RNA-seq aligner. Bioinformatics *29*, 15–21. https://doi.org/10.1093/bioinformatics/bts635.

Ehx, G., Larouche, J.D., Durette, C., Laverdure, J.P., Hesnard, L., Vincent, K., Hardy, M.P., Theriault, C., Rulleau, C., Lanoix, J., et al. (2021). Atypical acute myeloid leukemia-specific transcripts generate shared and immunogenic MHC class-I-associated epitopes. Immunity *54*, 737–752.e10. https://doi.org/10.1016/j.immuni.2021.03.001.

Forlani, G., Michaux, J., Pak, H., Huber, F., Marie Joseph, E.L., Ramia, E., Stevenson, B.J., Linnebacher, M., Accolla, R.S., and Bassani-Sternberg, M. (2021). CIITA-transduced glioblastoma cells uncover a rich repertoire of clinically relevant tumor-associated HLA-II antigens. Mol. Cell. Proteomics *20*, 100032. https://doi.org/10.1074/mcp.ra120.002201.

Garcia-Perez, J.L., Widmann, T.J., and Adams, I.R. (2016). The impact of transposable elements on mammalian development. Development *143*, 4101–4114. https://doi.org/10.1242/dev.132639.

Gromeier, M., Brown, M.C., Zhang, G., Lin, X., Chen, Y., Wei, Z., Beaubier, N., Yan, H., He, Y., Desjardins, A., et al. (2021). Very low mutation burden is a feature of inflamed recurrent glioblastomas responsive to cancer immunotherapy. Nat. Commun. *12*, 352. https://doi.org/10.1038/s41467-020-20469-6.

Grundy, E.E., Diab, N., and Chiappinelli, K.B. (2021). Transposable element regulation and expression in cancer. FEBS J. *289*, 1160–1179. https://doi.org/10.1111/febs.15722.

Gu, Z., Eils, R., and Schlesner, M. (2016). Complex heatmaps reveal patterns and correlations in multidimensional genomic data. Bioinformatics *32*, 2847–2849. https://doi.org/10.1093/bioinformatics/btw313.

Gubin, M.M., Zhang, X., Schuster, H., Caron, E., Ward, J.P., Noguchi, T., Ivanova, Y., Hundal, J., Arthur, C.D., Krebber, W.J., et al. (2014). Checkpoint blockade cancer immunotherapy targets tumour-specific mutant antigens. Nature *515*, 577–581. https://doi.org/10.1038/nature13988.

Harrow, J., Denoeud, F., Frankish, A., Reymond, A., Chen, C.K., Chrast, J., Lagarde, J., Gilbert, J.G.R., Storey, R., Swarbreck, D., et al. (2006). GENCODE: producing a reference annotation for ENCODE. Genome Biol. *7*, 1–9. https://doi.org/10.1186/gb-2006-7-s1-s4.

He, J., Babarinde, I.A., Sun, L., Xu, S., Chen, R., Shi, J., Wei, Y., Li, Y., Ma, G., Zhuang, Q., et al. (2021). Identifying transposable element expression dynamics and heterogeneity during development at the single-cell level with a processing pipeline scTE. Nat. Commun. *12*, 1456. https://doi.org/10.1038/s41467-021-21808-x.

Jin, Y., Tam, O.H., Paniagua, E., and Hammell, M. (2015). TEtranscripts: a package for including transposable elements in differential expression analysis of RNA-seq datasets. Bioinformatics *31*, 3593–3599. https://doi.org/10.1093/bioinformatics/btv422.

Kolde, R. (2019). Pheatmap: Pretty Heatmaps. R Package Version 1.0. 12. R Packag version 10 *8*.

Kong, Y., Rose, C.M., Cass, A.A., Williams, A.G., Darwish, M., Lianoglou, S., Haverty, P.M., Tong, A.J., Blanchette, C., Albert, M.L., et al. (2019). Transposable element expression in tumors is associated with immune infiltration and increased antigenicity. Nat. Commun. *10*, 5228. https://doi.org/10.1038/s41467-019-13035-2.

Kurscheid, S., Bady, P., Sciuscio, D., Samarzija, I., Shay, T., Vassallo, I., Criekinge, W.V., Daniel, R.T., van den Bent, M.J., Marosi, C., et al. (2015). Chromosome 7 gain and DNA hypermethylation at the HOXA10 locus are associated with expression of a stem cell related HOX-signature in glioblastoma. Genome Biol. *16*, 16. https://doi.org/10.1186/s13059-015-0583-7.

Lanciano, S., and Cristofari, G. (2020). Measuring and interpreting transposable element expression. Nat. Rev. Genet. *21*, 721–736. https://doi.org/10.1038/s41576-020-0251-y.

Laumont, C.M., Daouda, T., Laverdure, J.P., Bonneil, E., Caron-Lizotte, O., Hardy, M.P., Granados, D.P., Durette, C., Lemieux, S., Thibault, P., and Perreault, C. (2016). Global proteogenomic analysis of human MHC class I-associated peptides derived from non-canonical reading frames. Nat. Commun. *7*, 10238. https://doi.org/10.1038/ncomms10238.

Laumont, C.M., Vincent, K., Hesnard, L., Audemard, E., Bonneil, E., Laverdure, J.P., Gendron, P., Courcelles, M., Hardy, M.P., Cote, C., et al. (2018). Noncoding regions are the main source of targetable tumor-specific antigens. Sci. Transl. Med. *10*. https://doi.org/10.1126/scitranslmed.aau5516.

Lavie, L., Kitova, M., Maldener, E., Meese, E., and Mayer, J. (2005). CpG methylation directly regulates transcriptional activity of the human endogenous retrovirus family HERV-K(HML-2). J. Virol. *79*, 876–883. https://doi.org/10.1128/jvi.79.2.876-883.2005.

Le, D.T., Uram, J.N., Wang, H., Bartlett, B.R., Kemberling, H., Eyring, A.D., Skora, A.D., Luber, B.S., Azad, N.S., Laheru, D., et al. (2015). PD-1 blockade in tumors with mismatch-repair deficiency. N. Engl. J. Med. *372*, 2509–2520. https://doi.org/10.1056/NEJMoa1500596.

Lennerz, V., Fatho, M., Gentilini, C., Frye, R.A., Lifke, A., Ferel, D., Wolfel, C., Huber, C., and Wolfel, T. (2005). The response of autologous T cells to a human melanoma is dominated by mutated neoantigens. Proc. Natl. Acad. Sci. U S A *102*, 16013–16018. https://doi.org/10.1073/pnas.0500090102.

Li, H., Handsaker, B., Wysoker, A., Fennell, T., Ruan, J., Homer, N., Marth, G., Abecasis, G., Durbin, R., and Genome Project Data Processing, S. (2009). The sequence alignment/map format and SAMtools. Bioinformatics *25*, 2078–2079. https://doi.org/10.1093/bioinformatics/btp352.

Liao, Y., Smyth, G.K., and Shi, W. (2014). featureCounts: an efficient general purpose program for assigning sequence reads to genomic features. Bioinformatics *30*, 923–930. https://doi.org/10.1093/bioinformatics/btt656.

Lynch-Sutherland, C.F., Chatterjee, A., Stockwell, P.A., Eccles, M.R., and Macaulay, E.C. (2020). Reawakening the developmental origins of cancer through transposable elements. Front. Oncol. *10*, 468. https://doi.org/10.3389/fonc.2020.00468.

McGinnis, S., and Madden, T.L. (2004). BLAST: at the core of a powerful and diverse set of sequence analysis tools. Nucleic Acids Res. *32*, W20–W25. https://doi.org/10.1093/nar/gkh435.

McGrail, D.J., Pilie, P.G., Rashid, N.U., Voorwerk, L., Slagter, M., Kok, M., Jonasch, E., Khasraw, M., Heimberger, A.B., Lim, B., et al. (2021). High tumor mutation burden fails to predict immune checkpoint blockade response across all cancer types. Ann. Oncol. *32*, 661–672. https://doi.org/10.1016/j.annonc.2021.02.006.

Morotti, M., Albukhari, A., Alsaadi, A., Artibani, M., Brenton, J.D., Curbishley, S.M., Dong, T., Dustin, M.L., Hu, Z., McGranahan, N., et al. (2021). Promises and challenges of adoptive T-cell therapies for solid tumours. Br. J. Cancer *124*, 1759–1776. https://doi.org/10.1038/s41416-021-01353-6.

Nakagawa, S., and Takahashi, M.U. (2016). gEVE: a genome-based endogenous viral element database provides comprehensive viral protein-coding sequences in mammalian genomes. Database (Oxford) *2016*, baw087.

Neukirch, L., Nielsen, T.K., Laursen, H., Daradoumis, J., Thirion, C., and Holst, P.J. (2019). Adenovirus based virus-like-vaccines targeting endogenous retroviruses can eliminate growing colorectal cancers in mice. Oncotarget *10*, 1458–1472. https://doi.org/10.18632/oncotarget.26680.

Novellino, L., Castelli, C., and Parmiani, G. (2005). A listing of human tumor antigens recognized by T cells: march 2004 update. Cancer Immunol. Immunother. *54*, 187–207. https://doi.org/10.1007/s00262-004-0560-6.

Ohtani, H., Orskov, A.D., Helbo, A.S., Gillberg, L., Liu, M., Zhou, W., Ungerstedt, J., Hellstrom-Lindberg, E., Sun, W., Liang, G., et al. (2020). Activation of a subset of evolutionarily young transposable elements and innate immunity are linked to clinical responses to 5-azacytidine. Cancer Res. *80*, 2441–2450. https://doi.org/10.1158/0008-5472.can-19-1696.

Pittet, M.J., Valmori, D., Dunbar, P.R., Speiser, D.E., Lienard, D., Lejeune, F., Fleischhauer, K., Cerundolo, V., Cerottini, J.C., and Romero, P. (1999). High frequencies of naive Melan-A/MART-1-specific CD8(+) T cells in a large proportion of human histocompatibility leukocyte antigen (HLA)-A2 individuals. J. Exp. Med. *190*, 705–716. https://doi.org/10.1084/jem.190.5.705.

Quinlan, A.R., and Hall, I.M. (2010). BEDTools: a flexible suite of utilities for comparing genomic features. Bioinformatics *26*, 841–842. https://doi.org/10.1093/bioinformatics/btq033.

Ramirez, F., Dundar, F., Diehl, S., Gruning, B.A., and Manke, T. (2014). deepTools: a flexible platform for exploring deep-sequencing data. Nucleic Acids Res. *42*, W187–W191. https://doi.org/10.1093/nar/gku365.

Rapoport, A.P., Stadtmauer, E.A., Binder-Scholl, G.K., Goloubeva, O., Vogl, D.T., Lacey, S.F., Badros, A.Z., Garfall, A., Weiss, B., Finklestein, J., et al. (2015). NY-ESO-1-specific TCR-engineered T cells mediate sustained antigen-specific antitumor effects in myeloma. Nat. Med. *21*, 914–921. https://doi.org/10.1038/nm.3910.

Rizvi, N.A., Hellmann, M.D., Snyder, A., Kvistborg, P., Makarov, V., Havel, J.J., Lee, W., Yuan, J., Wong, P., Ho, T.S., et al. (2015). Cancer immunology. Mutational landscape determines sensitivity to PD-1 blockade in non-small cell lung cancer. Science *348*, 124–128. https://doi.org/10.1126/science.aaa1348.

Robbins, P.F., El-Gamil, M., Li, Y.F., Kawakami, Y., Loftus, D., Appella, E., and Rosenberg, S.A. (1996). A mutated beta-catenin gene encodes a melanoma-specific antigen recognized by tumor infiltrating lymphocytes. J. Exp. Med. *183*, 1185–1192. https://doi.org/10.1084/jem.183.3.1185.

Robbins, P.F., Lu, Y.C., El-Gamil, M., Li, Y.F., Gross, C., Gartner, J., Lin, J.C., Teer, J.K., Cliften, P., Tycksen, E., et al. (2013). Mining exomic sequencing data to identify mutated antigens recognized by adoptively transferred tumor-reactive T cells. Nat. Med. *19*, 747–752. https://doi.org/10.1038/nm.3161.

Robinson, J.T., Thorvaldsdottir, H., Wenger, A.M., Zehir, A., and Mesirov, J.P. (2017). Variant review with the integrative genomics viewer. Cancer Res. *77*, e31–e34. https://doi.org/10.1158/0008-5472.can-17-0337.

Rodic, N., Steranka, J.P., Makohon-Moore, A., Moyer, A., Shen, P., Sharma, R., Kohutek, Z.A., Huang, C.R., Ahn, D., Mita, P., et al. (2015). Retrotransposon insertions in the clonal evolution of pancreatic ductal adenocarcinoma. Nat. Med. *21*, 1060–1064. https://doi.org/10.1038/nm.3919.

Rooney, M.S., Shukla, S.A., Wu, C.J., Getz, G., and Hacohen, N. (2015). Molecular and genetic properties of tumors associated with local immune cytolytic activity. Cell *160*, 48–61. https://doi.org/10.1016/j.cell.2014.12.033.

Roulois, D., Loo Yau, H., Singhania, R., Wang, Y., Danesh, A., Shen, S.Y., Han, H., Liang, G., Jones, P.A., Pugh, T.J., et al. (2015). DNA-demethylating agents target colorectal cancer cells by inducing viral mimicry by endogenous transcripts. Cell *162*, 961–973. https://doi.org/10.1016/j.cell.2015.07.056.

Rycaj, K., Plummer, J.B., Yin, B., Li, M., Garza, J., Radvanyi, L., Ramondetta, L.M., Lin, K., Johanning, G.L., Tang, D.G., and Wang-Johanning, F. (2015). Cytotoxicity of human endogenous retrovirus K-specific T cells toward autologous ovarian cancer cells. Clin. Cancer Res. *21*, 471–483. https://doi.org/10.1158/1078-0432.ccr-14-0388.

Sacha, J.B., Kim, I.J., Chen, L., Ullah, J.H., Goodwin, D.A., Simmons, H.A., Schenkman, D.I., von Pelchrzim, F., Gifford, R.J., Nimityongskul, F.A., et al. (2012). Vaccination with cancer- and HIV infection-associated endogenous retrotransposable elements is safe and immunogenic. J. Immunol. *189*, 1467–1479. https://doi.org/10.4049/jimmunol.1200079.

Saini, S.K., Orskov, A.D., Bjerregaard, A.M., Unnikrishnan, A., Holmberg-Thyden, S., Borch, A., Jensen, K.V., Anande, G., Bentzen, A.K., Marquard, A.M., et al. (2020). Human endogenous retroviruses form a reservoir of T cell targets in hematological cancers. Nat. Commun. *11*, 5660. https://doi.org/10.1038/s41467-020-19464-8.

Sarkizova, S., Klaeger, S., Le, P.M., Li, L.W., Oliveira, G., Keshishian, H., Hartigan, C.R., Zhang, W., Braun, D.A., Ligon, K.L., et al. (2020). A large peptidome dataset improves HLA class I epitope prediction across most of the human population. Nat. Biotechnol. *38*, 199–209. https://doi.org/10.1038/s41587-019-0322-9.

Schadendorf, D., Hodi, F.S., Robert, C., Weber, J.S., Margolin, K., Hamid, O., Patt, D., Chen, T.T., Berman, D.M., and Wolchok, J.D. (2015). Pooled analysis of long-term survival data from phase II and phase III trials of ipilimumab in unresectable or metastatic melanoma. J. Clin. Oncol. *33*, 1889–1894. https://doi.org/10.1200/jco.2014.56.2736.

Scott, E.C., Gardner, E.J., Masood, A., Chuang, N.T., Vertino, P.M., and Devine, S.E. (2016). A hot L1 retrotransposon evades somatic repression and initiates human colorectal cancer. Genome Res. *26*, 745–755. https://doi.org/10.1101/gr.201814.115.

Shao, W., and Wang, T. (2021). Transcript assembly improves expression quantification of transposable elements in single-cell RNA-seq data. Genome Res. *31*, 88–100. https://doi.org/10.1101/gr.265173.120.

Shraibman, B., Barnea, E., Kadosh, D.M., Haimovich, Y., Slobodin, G., Rosner, I., Lopez-Larrea, C., Hilf, N., Kuttruff, S., Song, C., et al. (2018). Identification of tumor antigens among the HLA peptidomes of glioblastoma tumors and plasma. Mol. Cell. Proteomics *17*, 2132–2145. https://doi.org/10.1074/mcp.ra118.000792.

Shraibman, B., Kadosh, D.M., Barnea, E., and Admon, A. (2016). Human leukocyte antigen (HLA) peptides derived from tumor antigens induced by inhibition of DNA methylation for development of drug-facilitated immunotherapy. Mol. Cell. Proteomics *15*, 3058–3070. https://doi.org/10.1074/mcp.m116.060350.

Simpson, A.J.G., Caballero, O.L., Jungbluth, A., Chen, Y.T., and Old, L.J. (2005). Cancer/testis antigens, gametogenesis and cancer. Nat. Rev. Cancer *5*, 615–625. https://doi.org/10.1038/nrc1669.

Slotkin, R.K., and Martienssen, R. (2007). Transposable elements and the epigenetic regulation of the genome. Nat. Rev. Genet. *8*, 272–285. https://doi.org/10.1038/nrg2072.

Smith, C.C., Beckermann, K.E., Bortone, D.S., De Cubas, A.A., Bixby, L.M., Lee, S.J., Panda, A., Ganesan, S., Bhanot, G., Wallen, E.M., et al. (2018). Endogenous retroviral signatures predict immunotherapy response in clear cell renal cell carcinoma. J. Clin. Invest. *128*, 4804–4820. https://doi.org/10.1172/jci121476.

Snyder, A., Makarov, V., Merghoub, T., Yuan, J., Zaretsky, J.M., Desrichard, A., Walsh, L.A., Postow, M.A., Wong, P., Ho, T.S., et al. (2014). Genetic basis for clinical response to CTLA-4 blockade in melanoma. N. Engl. J. Med. *371*, 2189–2199. https://doi.org/10.1056/NEJMoa1406498.

Subramanian, A., Tamayo, P., Mootha, V.K., Mukherjee, S., Ebert, B.L., Gillette, M.A., Paulovich, A., Pomeroy, S.L., Golub, T.R., Lander, E.S., and Mesirov, J.P. (2005). Gene set enrichment analysis: a knowledge-based approach for interpreting genome-wide expression profiles. Proc. Natl. Acad. Sci. U S A *102*, 15545–15550. https://doi.org/10.1073/pnas.0506580102.

Tjeldnes, H., Labun, K., Torres Cleuren, Y., Chyzynska, K., Swirski, M., and Valen, E. (2021). ORFik: a comprehensive R toolkit for the analysis of translation. BMC Bioinf. *22*, 336. https://doi.org/10.1186/s12859-021-04254-w.

Tran, E., Ahmadzadeh, M., Lu, Y.C., Gros, A., Turcotte, S., Robbins, P.F., Gartner, J.J., Zheng, Z., Li, Y.F., Ray, S., et al. (2015). Immunogenicity of somatic mutations in human gastrointestinal cancers. Science *350*, 1387–1390. https://doi.org/10.1126/science.aad1253.

van der Bruggen, P., Traversari, C., Chomez, P., Lurquin, C., De Plaen, E., Van den Eynde, B., Knuth, A., and Boon, T. (1991). A gene encoding an antigen recognized by cytolytic T lymphocytes on a human melanoma. Science *254*, 1643–1647. https://doi.org/10.1126/science.1840703.

van Rooij, N., van Buuren, M.M., Philips, D., Velds, A., Toebes, M., Heemskerk, B., van Dijk, L.J., Behjati, S., Hilkmann, H., El Atmioui, D., et al. (2013). Tumor exome analysis reveals neoantigen-specific T-cell reactivity in an ipilimumab-responsive melanoma. J. Clin. Oncol. *31*, e439–442. https://doi.org/10.1200/jco.2012.47.7521.

Vita, R., Mahajan, S., Overton, J.A., Dhanda, S.K., Martini, S., Cantrell, J.R., Wheeler, D.K., Sette, A., and Peters, B. (2019). The immune epitope database (IEDB): 2018 update. Nucleic Acids Res. *47*, D339–D343. https://doi.org/10.1093/nar/gky1006.

Waldman, A.D., Fritz, J.M., and Lenardo, M.J. (2020). A guide to cancer immunotherapy: from T cell basic science to clinical practice. Nat. Rev. Immunol. *20*, 651–668. https://doi.org/10.1038/s41577-020-0306-5.

Wang-Johanning, F., Radvanyi, L., Rycaj, K., Plummer, J.B., Yan, P., Sastry, K.J., Piyathilake, C.J., Hunt, K.K., and Johanning, G.L. (2008). Human endogenous retrovirus K triggers an antigen-specific immune response in breast cancer patients. Cancer Res. *68*, 5869–5877. https://doi.org/10.1158/0008-5472.can-07-6838.

Wickham, H. (2016). ggplot2: Elegant Graphics for Data Analysis (Springer-Verlag).

Wickham, H., François, R., Henry, L., and Müller, K. (2022). Dplyr: A Grammar of Data Manipulation.

Wickham, H., and Girlich, M. (2022). Tidyr: Tidy Messy Data.

Yarchoan, M., Albacker, L.A., Hopkins, A.C., Montesion, M., Murugesan, K., Vithayathil, T.T., Zaidi, N., Azad, N.S., Laheru, D.A., Frampton, G.M., and Jaffee, E.M. (2019). PD-L1 expression and tumor mutational burden are independent biomarkers in most cancers. JCI Insight *4*, e126908. https://doi.org/10.1172/jci.insight.126908.

Yarchoan, M., Hopkins, A., and Jaffee, E.M. (2017). Tumor mutational burden and response rate to PD-1 inhibition. N. Engl. J. Med. *377*, 2500–2501. https://doi.org/10.1056/nejmc1713444.

Zhao, Q., Laverdure, J.P., Lanoix, J., Durette, C., Cote, C., Bonneil, E., Laumont, C.M., Gendron, P., Vincent, K., Courcelles, M., et al. (2020). Proteogenomics uncovers a vast repertoire of shared tumor-specific antigens in ovarian cancer. Cancer Immunol. Res. *8*, 544–555. https://doi.org/10.1158/2326-6066.cir-19-0541.

CellPress
OPEN ACCESS

STAR★METHODS

KEY RESOURCES TABLE

REAGENT or RESOURCE	SOURCE	IDENTIFIER
Antibodies		
BV711 Streptavidin	BD Biosciences	Cat# 563262; RRID:AB_2869478
APC Streptavidin	BD Biosciences	Cat# 554067; RRID:AB_10050396
FITC Streptavidin	BD Biosciences	Cat# 554060; RRID:AB_10053373
PE Streptavidin	BD Biosciences	Cat# 554061; RRID:AB_10053328
BV421 Streptavidin	BD Biosciences	Cat# 563259; RRID:AB_2869475
PE-CF594 Streptavidin	BD Biosciences	Cat# 562284; RRID:AB_11154598
PE-Cy5 Streptavidin	BD Biosciences	Cat# 554062; RRID:AB_10053563
PE Mouse Anti-Human HLA-A2 (Clone BB7.2)	BD Biosciences	Cat# 558570; RRID:AB_647220
PE Mouse IgG2b κ isotype	BD Biosciences	Cat# 555743; RRID:AB_396086
PE-Cy7 Mouse Anti-Human CD8 (Clone RPA-T8)	BD Biosciences	Cat# 557746; RRID:AB_396852
BV650 Mouse Anti-Human CD3 (Clone HIT3)	BD Biosciences	Cat# 740562; RRID:AB_2740263
BV605 Mouse Anti-Human CD4 (Clone OKT4)	Biolegend	Cat# 317438; RRID:AB_11218995
APC anti-human HLA-B7 Antibody (clone BB7.1)	Biolegend	Cat# 372405; RRID:AB_2650775
PE Anti-human β2-microglobulin (Clone BBM.1)	Santa Cruz	Cat# sc-13565; RRID:AB_626748
Biological samples		
Human peripheral blood	Etablissement Français du Sang	Paris, France
Chemicals, peptides, and recombinant proteins		
Bovine Serum Albumin	SIGMA	A7906
X-VIVO 15 Serum-free Hematopoietic Cell Medium	Lonza	BE02-060F
Penicillin-Streptomycin	Gibco	15070063
Synthetic peptides	Genecust	N/A
Proleukin (IL-2)	Novartis	Proleukin SC
Lymphoprep	StemCell	07851
Human GM-CSF	Miltenyi	130-093-864
Human IL4	Miltenyi	130-093-922
Recombinant Human IL7	Preprotech	200-07
Critical commercial assays		
Easymer HLA-A*02:01	Immunaware	1002-01
Easymers HLA-B*07:02	Immunaware	1048-01
CD8 MicroBeads, human	Miltenyi	Cat# 130-045-201; RRID:AB_2889920
CD4 MicroBeads, human	Miltenyi	Cat# 130-045-101; RRID:AB_2889919
CD14 MicroBeads, human	Miltenyi	Cat# 130-050-201; RRID:AB_2665482
Streptavidin coated beads	Spherotech	SVP-60-5
LIVE/DEAD™ Fixable Aqua Dead Cell Stain Kit	Thermo Fischer Scientific	L34957
Fetal Calf Serum	Eurobio	CVFSVF00-01
Deposited data		
Mass spectrometry raw data from GBM CIITA+ cell line immunopeptidomics	(Forlani et al., 2021)	PRIDE: PXD020079
Mass spectrometry raw data from GBM tumor immunopeptidomics	(Shraibman et al., 2018)	PRIDE: PXD008127
Mass spectrometry raw data from GBM decitabine treated cell line immunopeptidomics	(Shraibman et al., 2016)	PRIDE: PXD003790
Mass spectrometry raw data from GBM immunopeptidomics	(Sarkizova et al., 2020)	MASSIVE: MSV000084442
Raw data files for GBM single-cell SMART-Seq2 data	(Darmanis et al., 2017)	GEO: GSE84465

(*Continued on next page*)

Continued		
REAGENT or RESOURCE	SOURCE	IDENTIFIER
Raw data files for TCGA GBM Bulk RNA-seq data	(Brennan et al., 2013)	https://portal.gdc.cancer.gov/legacy-archive
Raw data files for GTEx Bulk RNA-seq data	(Consortium, 2013)	https://www.ncbi.nlm.nih.gov/projects/gap/cgi-bin/study.cgi?study_id=phs000424.v8.p2
Software and algorithms		
Proteome Discoverer 2.5	ThermoFisher	OPTON-31040
GibbsCluster 2.0	DTU Health Tech	https://services.healthtech.dtu.dk/service.php?GibbsCluster-2.0
NetMHC 4.0	DTU Health Tech	https://services.healthtech.dtu.dk/service.php?NetMHC-4.0
R 3.6.3	R	https://www.r-project.org/
R 4.0.3	R	https://www.r-project.org/
RStudio	RStudio	https://www.rstudio.com/
Pheatmap	(Kolde, 2019)	https://cran.r-project.org/web/packages/pheatmap/index.html
ComplexHeatmap	(Gu et al., 2016)	https://www.bioconductor.org/packages/release/bioc/html/ComplexHeatmap.html
ggplot2	(Wickham, 2016)	https://cran.r-project.org/web/packages/ggplot2/index.html
Tidyr	(Wickham and Girlich, 2022)	https://github.com/tidyverse/tidyr
Dplyr	(Wickham et al., 2022)	https://github.com/tidyverse/dplyr
ORFik	(Tjeldnes et al., 2021)	http://bioconductor.org/packages/release/bioc/html/ORFik.html
Bedtools	(Quinlan and Hall, 2010)	https://bedtools.readthedocs.io/en/latest/
Deeptools	(Ramirez et al., 2014)	https://deeptools.readthedocs.io/en/develop/
Seurat	(Butler et al., 2018)	www.satijalab.org/seurat/
FeatureCounts	(Liao et al., 2014)	http://subread.sourceforge.net/
STAR	(Dobin et al., 2013)	https://github.com/alexdobin/STAR
Samtools	(Li et al., 2009)	http://samtools.sourceforge.net/
GSEA	(Subramanian et al., 2005)	https://www.gsea-msigdb.org/gsea/index.jsp
Lift Genome annotations	UCSC	https://genome.ucsc.edu/cgi-bin/hgLiftOver
Blast	(McGinnis and Madden, 2004)	https://blast.ncbi.nlm.nih.gov/Blast.cgi
IGV	(Robinson et al., 2017)	https://software.broadinstitute.org/software/igv/
Other		
Script to annotate ORFs on TE sequences	This paper	Mendeley (https://doi.org/10.17632/23b45jkb29.1)
Homer annotations	Benner lab	http://homer.ucsd.edu/homer/
Gencode gene annotations	(Harrow et al., 2006)	https://www.gencodegenes.org/human/release_19.html
TEtranscripts TEs annotations	(Jin et al., 2015)	http://hammelllab.labsites.cshl.edu/software
gEVE TEs annotations	(Nakagawa and Takahashi, 2016)	http://geve.med.u-tokai.ac.jp/

RESOURCE AVAILABILITY

Lead contact

Further information and requests for resources and reagents should be directed to and will be fulfilled by the Lead Contact, Sebastian Amigorena (sebastian.amigorena@curie.fr) and Christel Goudot (christel.goudot@curie.fr).

Materials availability

This study did not generate new unique reagents.

Data and code availability

All data used in the paper are listed in the key resources table.

All original code has been deposited at Mendeley and is publicly available as of the date of publication. DOIs are listed in the key resources table.

Any additional information required to reanalyze the data reported in this paper is available from the lead contact upon request.

EXPERIMENTAL MODEL AND SUBJECT DETAILS

Human research participants

Buffy coats from healthy donors were obtained from Etablissement Français du Sang (Paris, France) in accordance with INSERM ethical guidelines. According to French Public Health Law (art L 1121-1-1, art L 1121-1-2), written consent and IRB approval are not required for human non-interventional studies.

In-vitro vaccinations assay

PBMCs were obtained by density gradient separation using Lymphoprep (StemCell Technologies) and phenotyped by FACS using anti-HLA-A2 (clone BB7.2, BD Biosciences) and anti-HLA-B7 antibodies (clone BB7.1, Biolegend). Only HLA-A2+ and/or HLA-B7+ donors were used.

Monocytes and lymphocytes from the same donor were purified as CD14+, CD4+ and CD8+ cells, respectively, by positive selection using magnetic beads (Miltenyi Biotec). Monocyte-derived dendritic cells (mo-DCs) were obtained by differentiation of CD14 + fraction during 5 days at 10^6 cells/mL in RPMI-1650/Glutamax (Gibco), 10% FBS, penicillin (100 U/mL)/streptomycin (100 μg/mL), recombinant human IL-4 (50ng/mL, Miltenyi Biotec) and GM-CSF (10ng/mL, Miltenyi Biotec). Isolated CD4+ and CD8+ T cells were cryopreserved after purification.

After differentiation, mo-DCs were seeded in 24 well plates at 1×10^6 cells/mL and maturated overnight with LPS (100 ng/mL). Then, culture media was removed, and LPS treated mo-DCs were pulsed during 3h at 37°C with a mix of selected good-binder TE-derived peptides (either predicted or from HLA-I peptidomic data). Each peptide was added at 1 μg/mL final concentration. Finally, peptide-loaded mo-DCs were harvested, pelleted and counted.

Cryopreserved lymphocyte fractions were thawed, and co-cultures were performed by mixing 1×10^6 CD8+ T cells, $0{,}1 \times 10^6$ CD4+ T cells and $0{,}1 \times 10^6$ peptide-loaded mo-DCs (CD8-CD4-mo-DCs ratio: 10:1:1, respectively) in a final volume of 2mL in 24 well plate. Each well was considered as an independent replicate. Total number of replicates was limited by the total number of CD8+ T cells. Without disturbing the cells, half of the media was changed after 5 days and then, the culture was monitored every 3 days until day 15-20. Expansion of specific CD8+ T cell populations was evaluated by FACS using tetramer staining.

X-vivo 15 medium (Lonza) supplemented with penicillin (100 U/mL)/streptomycin (100 μg/mL) (Gibco), 10% FBS, IL-2 (10 U/mL, Novartis) and IL-7 (10 ng/mL, PeproTech) was used as culture media.

As negative control, a replicate using non-peptide pulsed mo-DCs was included. For HLA-A2+ donors, a positive control of T cell expansions (1 or 2 replicates) using mo-DCs pulsed with mutated Melan-A peptide (ELAGIGILTV) was included. 3 HLA-A*02:01 binding peptides derived from normal proteins were included.

Peptide binding to HLA-A*02:01 and HLA-B*07:02 by tetramer formation.

Predicted peptides were synthetized by GeneCust with a >98% purity. HLA-A*02:01 and HLA-B*07:02 monomers were purchased as easYmers from Immunaware (Copenhagen, Denmark). The binding to HLA-A*02:01 and HLA-B*07:02 of the predicted and MSTE-derived peptides was measured by HLA-I-tetramer complex formation following manufacturer's instructions. Briefly, biotinylated monomers were incubated with synthetic peptides (100 mM) at 18°C during 48h. Then, they were bound to streptavidin-coated beads and stained with PE-conjugated anti-β2-microglobulin antibody. As positive controls for HLA-A*0201-complex formation, CMV pp65 495-503 (NLVPMVATV) and mutated Melan-A (ELAGIGILTV) were used. CMV pp65 417-426 (TPRVTGGGAM) peptide was used for HLA-B*07:02. Binding is represented as percentage of HLA-I-complex formation relative to CMV positive controls. Peptides with HLA-I-complex formation of at least 50% relative to positive control were used in *in-vitro* vaccination experiments.

For tetramer formation, peptide-HLA-I-complexes were tetramerized using different fluorescent streptavidins (PE, APC, BV421, BV711, PE-CF549 and PECy5) at a final concentration of 8 mg/mL. All tetramers were kept at 4°C and used within 2 months.

Tetramer staining and analysis

Tetramer staining was performed on total cells after in-vitro vaccination experiments by combining 1μL of each tetramer specificity, and two different streptavidin-labelled tetramers per specificity. The staining was performed during 20 min at RT in a final volume of 100 μL of PBS 1% BSA per 1M cells. Then, 100 μL of surface antibody mix containing anti-CD3 BV650 (BD Biosciences) and anti-CD8 PECy7 (BD Biosciences) at 1/200 final dilution was added and incubated for further 20 min at 4°C. Finally, cells were washed twice with PBS-1% BSA and analyzed by flow cytometry. Live/Dead Aqua-405nm (ThermoFisher) was used to exclude dead cells. Data was collected using a ZE5 Cell Analyzer (Bio-Rad) and analyzed using FlowJo v10.3.

Tetramer analysis was done on live, single cells, CD3+CD8+ cells following the strategy described by Andersen et al. (Andersen et al., 2012). Expansions were considered positive when positive for both streptavidin-labelled tetramers. Expanded populations for each peptide are represented either as frequencies of total CD8+ cells in each replicate or as total tetramer frequencies among total CD8+ T cells evaluated in all replicated for one donor.

METHOD DETAILS

Transposable element annotations

Classification and TE metadata

Transposable Element annotations have been retrieved from two different databases: from Homer repeat gtf annotation file (v4.11.1) based on hg19 (v6.4) UCSC annotations, and from TEtranscript (Jin et al., 2015) hg19 gtf annotation file. Both annotations are based on RepeatMasker database and have been merged based on identical coordinates (Chr, Start, End) to obtain following information on each repeat: Class, Family, Subfamily, Divergence, coordinates. L1 family was subdivided into 2 families: (1) “L1PA/B/x” that include TEs from closely related L1HS, L1PA(x), L1PB(x), L1P(x) subfamilies; and (2) “Other L1” regrouping all other L1 that are not present in “L1PA/B/x”. All DNA transposons were classified as DNA. annotatePeaks.pl from Homer was performed to obtain genomic locations (intron, exon, 3′UTR, 5′UTR, intergenic, other) for each individual TE. Closest and intersect tools from bedtools (v2.29.2) have been used to retrieve, for each TE, the distance from closest protein-coding genes from gencode gtf annotation file (Release 19 GRCh37.p13) (Harrow et al., 2006).

Age of TEs

Repeat age was calculated using percentage of divergence for human repeats: Divergence/($2.2 * 10^{-9}$), following the formula from this article (Choudhary et al., 2020).

Ancient viral protein motif identification

Open reading frame (ORF) locations from Endogenous Viral Elements (EVE) were retrieved from gEVE database. As analyses were performed on human genome version hg19, hg38 gEVE annotations were formatted and adjusted to hg19 using “Lift Genome annotations” tool from UCSC available here: https://genome.ucsc.edu/cgi-bin/hgLiftOver. ORFs coordinates from gEVE annotations and from all individual TEs in the genome were matched to assign an EVE ORF to individual TEs in case of coordinate overlap. 30517 individual TEs overlapped an EVE ORF, with most of them being L1 (mostly L1PA/B/x) and ERV (mostly ERV1, ERVK, ERVL) elements. To identify amino acid sequence similarity between canonical TE proteins from gEVE database and peptides from immunopeptidomics, a blastp (McGinnis and Madden, 2004) was performed between gEVE protein sequences and the immunopeptidomic sequences. No threshold on Evalue was set, and the similarity was estimated and classified in 3 categories: (1) 100% match: no mismatch, no gap and query coverage per HSP to 100%; (2) at most 1 mismatch: 1 mismatch, no gap and query coverage per HSP above 85%; and (3) at most 2 mismatches: 2 mismatches, no gap and query coverage per HSP above 85%.

Analysis of known TE proteins

LTR and LINE proteins

LTRs coding for peptides overlapping an intact ORF were classified as Env, Gag, Pol or Pro using RetroTector annotations from gEVE. For LINE elements, a blastp (v2.12.0+) was performed between LINE-derived peptides and either ORF1p and ORF2p protein sequences found in Uniprot (accession numbers Q9UN81 and O00370). LINE and LTR coding for a peptide were also compared to gEVE HMM profile annotations to classify the TE protein motif found in those TEs.

TE ORF annotations

A homemade R script was used to identify and annotate ORFs from TE sequences. (1) TE nucleotide sequences were formatted to obtain 6 frames using R package Biostrings (v2.58.0) and its functions DNAStringSet and reverseComplement. (2) 6-frame sequences were translated with translate function from Biostrings. (3) Stop codons and methionines were detected using matchPDict function from Biostrings. (4) Peptides from immunopeptidomics were mapped using matchPDict function. (5) ORFik R package (v1.10.13) (Tjeldnes et al., 2021) was used to detect ORF with at least 30bp (3 for the start codon, 8AA*3 for the sequence, 3 for the stop codon) and to keep only the longest ORF. Two different start codon patterns were submitted to detect ORFs: “ATG” for canonical start codons and “ATG|CTG|GTG|TTG” for canonical and non-canonical start codons. ORFs only found using the second pattern were classified as “CTG|GTG|TTG”. (6) Length of ORFs were calculated using start and end positions. (7) R package ggplot2 was used to represent all identified ORFs, stop codons, methionines and peptide locations in all 6 frames of the TEs.

Single-cell data analysis

Downloading data and read alignment to genome

Smart-seq2 data (GEO accession number: GSE84465) were downloaded from the Sequence Read Archive (SRA) database using prefetch from SRA Toolkit (v2.10.0). SRA files were converted to fastq files using fastq-dump. Fastq files were 75bp paired-end unstranded reads. Raw RNA reads were mapped to the human genome (hg19) using the 2-pass mode of STAR (version 2.7.1.a) (Dobin et al., 2013) (parameters: –quantMode GeneCounts, –twopassMode Basic, –alignSJDBoverhangMin 1, –bamRemoveDuplicatesType UniqueIdentical, –winAnchorMultimapNmax 1000, –outFilterMultimapNmax 1000, –outFilterScoreMinOverLread

0.33, –outFilterMatchNminOverLread 0.33, –outFilterMismatchNoverLmax 0.04, –outMultimapperOrder Random, –sjdbOverhang 76).

Quantification of gene and TE expression

To compute quantification of TE and gene expression, featureCounts (Liao et al., 2014) from Subread (v1.6.4) was computed on each genome-mapped read files. Different parameters were used depending on the analysis : (1) for gene expression : –p –ignoreDup –g gene_id using gencode gtf annotation file; (2) for TE expression on individual copies (a) considering only uniquely mapping reads: –p –ignoreDup –g transcript_id using TEtranscript hg19 gtf annotation file; (b) considering uniquely and multi-mapping reads : –p –ignoreDup –g transcript_id -M –primary; (3) for TE expression on subfamilies with uniquely and multi-mapping reads : –p –ignoreDup –g gene_id -M –primary. Cell count files were merged into a matrix with a homemade python script (Python 3.6).

Filtering features and cells, normalization and batch correction

Cell metadata and feature raw count matrices were imported to R (v4.0.3) to create a SingleCellExperiment R object. CPM, FPKM and TPM values on gene and TE expression were calculated on raw counts prior to any filtering using scuttle R package (v1.0.4) and its functions: calculateCPM, calculateFPKM, calculateTPM. Cells with low number of counts and low number of features (3 times lower than MAD) were removed using Scater and Scran packages. To remove low expressed features, several filters have been applied depending on the analysis. For TE expression using uniquely-mapped reads (1), individual TEs with less than 1 count/cell in average were removed [22000 individual remaining TEs]. For TE expression using multi-mapped reads (2), individual TEs with less than 5 counts in at least 20 cells were removed to take into account expression in small populations [130028 individual TEs]. For gene expression (3), genes with less than 5 counts in at least 20 cells were removed [19867 genes remaining]. For TE subfamily expression, no filtering was performed [992 subfamilies]. Raw count matrices were then normalized using logNormCounts function from scater R package. After several verifications, a batch effect linked to the plate ID of the cells was identified. To correct it, removeBatchEffect function from limma R package was used providing the plate ID as batch and the cell type as design.

Dimensionality reduction

A single Seurat object was created importing raw, normalized and normalized + corrected feature matrices into different assays. CPM, FPKM and TPM matrices were also imported. Seurat v3 was used for the uniquely mapped read analysis; Seurat v4 was used for the multi-mapped read analysis, the subfamily analysis and the gene analysis. From Seurat, FindVariableFeatures was performed to distinguish the 5,000 most variable genes or individual TEs; ScaleData to scale feature expression, RunPCA to compute 75 Principal Components, RunTSNE to perform t-SNE dimension reduction on 50 Principal Components. Dimensionality reduction step was performed on normalized + corrected assay.

Differential expression analysis and enrichment tests

From Seurat, FindAllMarkers was performed on annotated cell types with a threshold of 0.25 foldchange (either natural log with Seurat v3 or log2 with v4) on features expressed in at least 10% of all cells in 1 cell type. Genes, subfamily and individual TE signatures were designed based on FindAllMarkers results using differentially expressed features with an adjusted p value lower or equal to 0.05. Signature scores were computed with the Seurat function AddModuleScore using the feature signature of interest. This function calculates, for each individual cell, the average expression of each feature from the signature, subtracted by the aggregated expression of control feature sets. TE subfamily enrichment was performed using all annotated individual TEs in the genome (4.6 million TEs) as a reference and either all expressed TEs or individual TE signatures from each population as ours queries. A hypergeometric test was computed using phyper from stats R package (v4.0.3). Then, a False Discovery Rate correction was applied using p.adjust from stats R package.

Radarplot and chromosome distribution

Radarplots representing feature distribution on chromosomes were made using radarchart function from fmsb R package (v0.7.1). Genomic proportions were calculated using all annotated genes and individual TEs from gencode and TEtranscript annotations, respectively.

Bulk RNA-seq data analysis

Downloading, alignment to genome and quantification

Around 50 samples from each GTEx tissue (Consortium, 2013) were randomly targeted and their fastq read files were downloaded using prefetch and fasterq-dump from sratoolkit (v2.10.0). Fastq reads from TCGA-GBM project (Brennan et al., 2013) were downloaded using gdc-client (v1.6.1). Alignment and feature quantification (genes, individual TEs, TE subfamilies) were done in the same protocol described for the Smart-seq2 analysis. Expression was normalized using estimateSizeFactors from DESeq2 R package (v1.30.1) to obtaine normalized counts. TPM values were also computed using calculateTPM function from scuttle. Two subsets of TE expression matrices were obtained for each database: (1) Expression matrices with only TEs from the neoplastic single-cell TE signatures; (2) Expression matrices with only expressed TEs. TEs were considered as expressed if we could observe at least 5 counts for 20% or more of the samples (considering separately either all samples from TCGA or GTEx database). 130640 TEs were retained for the TCGA samples whereas 192243 TEs were kept for the GTEx samples. Among those, 103585 TEs were common to both databases.

Downstream analysis of bulk RNA-seq samples

Merged neoplastic signature specific matrix with all samples from TCGA and GTEx was imported in a Seurat object. DESeq2 normalized counts and TPM values were both imported. Using normalized counts, ScaleData, RunPCA and RunUMAP were applied to obtain UMAP representations. To assess signature expression in the samples, median expression of all TEs from the neoplastic signature was done using TPM values.

Gene set enrichment analysis

Gene Set Enrichment Analysis (GSEA) (Subramanian et al., 2005) was performed using DESeq2 normalized count matrices of common expressed TEs between TCGA and GTEx databases (103585 TEs) to test enrichment of neoplastic single-cell signature in either Normal or Tumor samples. GSEA (v4.2.1) was run with default parameters. GSEA results were imported to R and ggplot2 was used to make representations.

Mass spectrometry based immunopeptidomics

Mass spectrometry data analysis

MS-based immunopeptidomic files were obtained from PXD020079, PXD008127, PXD003790 and MSV000084442. They were analysed with ProteomeDiscoverer 2.5 (ThermoFisher) using the following parameters: no-enzyme, precursor mass tolerance 20ppm and fragment mass tolerance 0.02 Da. Methionine oxidation and N-acetylation were enabled as variable modifications. Using Percolator, a false discovery rate (FDR) of 1% was applied at peptide level and no FDR was used at protein level. Spectra were searched against the human Uniprot/SwissProt with isoforms (updated 06/03/2020) concatenated with the 6 reading frame in silico translated neoplastic enriched TE database (from uniquely- or multiple-mapped analysis). Identified potential TE-derived peptides were filtered afterwards with UniProt/TrEMBL database, considering leucine-isoleucine and lysine-glutamine as equivalent, respectively. Finally, spectrums from TE-derived peptides were manually verified.

Peptide hydrophobicity index (HI) calculation

For retention time versus hydrophobicity comparisons, HI was predicted using SSRCalc web server (http://hs2.proteome.ca/SSRCalc/SSRCalcX.html).

Single and all assignments definition

As multiple TEs can code for the same peptides, we made two different categories to make observations on TE-encoded peptide features. *All assignments* correspond to all TEs coding for a peptide (all 568 TEs for 370 peptides). *Single assignment* corresponds to a random selection for each peptide of an individual TE that can encode the corresponding peptide (370 TEs for 370 peptides).

Identifying potential peptide-coding TEs

To identify all TEs coding for peptides identified with immunopeptidomic results, peptide amino acid sequences were aligned to all annotated individual TEs in the genome in all 6 reading frames using tblastn (v2.11.0+). Sequences from all TEs in the genome were retrieved using getfasta from bedtools (v2.30.0) (Quinlan and Hall, 2010) with TETranscript gtf processed into BED format. No restriction on Evalue was requested. All hits with a number of mismatches equal to 0, a number of gap openings equal to 0 and a query coverage per HSP of 100 were kept and considered as peptide-coding TEs in addition to those from the neoplastic signature identified with ProteomeDiscoverer.

Spectrum validation with synthetic peptides

To validate the spectra, 24 of the identified peptides were synthesized (GeneCust) with an HPLC purity of 95% and were injected in a Velos Orbitrap (CID or HCD). Raw files were analysed with ProteomeDiscoverer 2.5 (ThermoFisher). Spectrums were exported and compared to the spectrums derived from the immunopeptidomic analysis. Only PSM with the same charge between synthetic and endogenous and without modifications were analysed. The same fragmentation type (CID or HCD) between both spectrums was prioritized when possible.

Assessing related RNA expression of TE-derived peptides

Identification of tumor-enriched TE-derived peptides

TPM expression of all possible TEs from the genome that can potentially code for the identified peptides was retrieved, and 90^{th} percentile values were calculated for each tissue. TEs coding for each specific peptide were selected and their 90^{th} percentile values were summed to obtain the total transcript expression related to these peptides. For single-TE encoded peptides, related transcript expression was directly the 90^{th} percentile value of the TE coding for the peptides. A log2 ratio was then performed between peptide related expression in GBM samples compared to each GTEx tissue to assess if the related expression of these peptides were higher in GBM samples compared Normal tissues. Using median TPM expression in GBM samples as a threshold, the percentage of expression in normal samples with an equal or higher expression was also calculated for each tissue. Pheatmap function from ComplexHeatmap R package (v2.6.2) was then used to represent the log2 ratio, the 90th percentile values as well as the percentage of expression in normal samples. Clustering method used in the heatmap with the log2 ratio was ward.D2.

QUANTIFICATION AND STATISTICAL ANALYSIS

Figures

Most figures were made using R (v4.0.3). Piecharts, lollipop charts, barplots, violin plots, boxplots, jitterplots, volcano plots, density plots, scatterplots and dimensionality reduction plot were made using either ggplot2 R package (v3.3.3) (Wickham, 2016) or functions from Seurat package (Butler et al., 2018). Pie donut chart was made with PieDonut function from webR package (v0.1.6). Heatmaps were built with Pheatmap R package (v1.0.12) (Kolde, 2019) and ComplexHeatmap (v2.6.2) (Gu et al., 2016). Clustering method used was ward.D2. IGV (v2.8.10) (Robinson et al., 2017) was used to visualize read coverage of bulk RNA-seq samples.

Statistical analyses

Wilcoxon tests were performed with R package ggpubr (version 0.4.0) and its function stat_compare_means (1) to compare distance to closest gene between Immune and Neoplastic signatures; (2) to compare mean expression of the neoplastic signature in bulk RNA-seq samples; and (3) to compare length of canonical and non-canonical TE-derived peptides ORFs. Pearson correlation scores were computed using stat_cor from ggpubr: (1) to assess the correlation between TEs and their closest protein-coding gene; and (2) to assess the correlation between median age of TEs coding for a peptide and the number of TEs that can code for the peptide. Two proportions z-test were computed to compare LINE proportions in different subsets of individual TEs. The correspondence between p values and symbols is as follows: ns: $p > 0.05$; *: $p \leq 0.05$; **: $p \leq 0.01$; ***: $p \leq 0.001$; ****: $p \leq 0.0001$.